

Ultraviolet Spectroscopy and UV Lasers

edited by

Prabhakar Misra

*Howard University
Washington, D.C.*

Mark A. Dubinskii

*Magnon, Inc.
Reisterstown, Maryland*



MARCEL DEKKER, INC.

NEW YORK · BA SEL

Copyright © 2001 by Marcel Dekker, Inc. All Rights Reserved.

MARCEL DEKKER, INC.



Register now on dekker.com and receive a discount coupon towards your next Dekker purchase. Registered users enjoy these advantages:

- ✓ Preview content online for free
- ✓ Quickly access your subscriptions and downloads
- ✓ Sign up for email notifications about new products and special offers in your subject of interest

Send your book order to your regular book supplier or directly to your nearest Marcel Dekker, Inc. office:

USA, Canada, South America:

5 Ways to Order

- 🌐 **Website:** www.dekker.com
- ☎ **Toll-free:** 1-800-228-1160
- 📠 **Fax:** 1-845-796-1772
- ✉ **E-mail:** bookorders@dekker.com
- ✉ **Mail:** Marcel Dekker, Inc., Cimarron Road
P.O. Box 5005, Monticello, NY 12701-5185

Europe, Africa, Middle East Far East, Australia, India, China:

5 Ways to Order

- 🌐 **Website:** www.dekker.com
- ☎ **Phone:** +41-061-260-6300
- 📠 **Fax:** +41-061-260-6333
- ✉ **E-mail:** intlorders@dekker.com
- ✉ **Mail:** Marcel Dekker, AG
Hutgasse 4, Postfach 812
CH-4001 Basel, Switzerland

Please include quantity, ISBN, author, title, shipping and billing addresses, telephone number/fax number/e-mail address, method of shipment, and purchase order numbers or credit card information.

To purchase offprints of chapters that appear in any Marcel Dekker, Inc. book or reprints of articles that appear in any Marcel Dekker, Inc. journal:

offprints@dekker.com

To inquire about special sales and bulk purchases of Marcel Dekker, Inc. books or journals:

bulksale@dekker.com

research + dekker.com → results

8

VUV Laser Spectroscopy of Trivalent Rare-Earth Ions in Wide Band Gap Fluoride Crystals

Evangelia Sarantopoulou and Alciviadis-Constantinos Cefalas

*National Hellenic Research Foundation, Theoretical and Physical
Chemistry Institute, Athens, Greece*

I. INTRODUCTION

The absorption and the excitation spectroscopic characteristics of trivalent rare-earth (RE) ions in the vacuum ultraviolet (VUV) and ultraviolet (UV) spectral regions, activated in wide band gap fluorine dielectric crystals, are due to transitions between the levels of the $4f^n$ single electronic configuration of the trivalent RE ion, and the levels of the $4f^{n-1}5d$ mixed electronic configuration, where a $4f$ electron is promoted to a $5d$ localized level [1–3]. The $4f^n \leftrightarrow 4f^{n-1}5d$ electronic transitions are characterized by strong Frank–Condon factors with broadband absorption and emission spectra in the VUV and UV. In contrast, the intraconfigurational $4f^n \rightarrow 4f^n$ transitions are parity forbidden. They are forced by the crystal field configuration mixing and they appear to be weak and sharp.

There are two different experimental methods for exciting a trivalent RE ion in wide band gap dielectric crystals. The first method uses VUV lasers [4] and/or x-ray or synchrotron radiation [5,6]. This pumping arrangement has the advantage of populating the levels of the $4f^{n-1}5d$ electronic configuration directly from the ground state of the trivalent RE ion, via one photon transition only. The subsequent de-excitation mechanisms within the $4f^{n-1}5d$ electronic configuration efficiently populate the levels of the $4f^n$ single electronic configuration of the trivalent RE ion [7–9]. They allow one to study the excitation dynamics and the structure of the levels of the $4f^{n-1}5d$ electronic configuration of the trivalent RE

ions. The second method applies upconversion pumping arrangement with all solid state laser elements [10–12], which greatly simplifies the experimental obstacles arising from the VUV pumping. The radiative interconfigurational d–f transitions of the RE activated ions, in the wide band gap of dielectric crystals, offer the possibility that these materials can be used in a variety of applications and for generating coherent VUV or UV light. This is attractive due to its relative simplicity in comparison to existing nonlinear methods using gases and molecules. In the case of optically pumped $\text{LiYF}_4:\text{Ce}^{3+}$ and $\text{LaF}_3:\text{Ce}^{3+}$ crystals [13–15], laser emission at 325 and 286 nm was obtained, respectively. Waynant and Klein [16,17] have reported the first laser action in the VUV from solid-state dielectric crystals. They used the $\text{LaF}_3:\text{Nd}^{3+}$ dielectric crystal to generate laser action at 172 nm when it was optically pumped by incoherent light (emitted from excited Kr_2^* molecules). With a different pumping arrangement using an F_2 pulsed discharge molecular laser operating at 157.6 nm, coherent light from the same crystal at 172 nm was generated [18]. Fluorescent materials based on RE ions can also be used as high quantum efficiency phosphors [19], for plasma display screens and mercury-free light tubes [20–22], fast scintillators [23,24] and for light wave communications [25,26].

In addition to the above-mentioned applications, next-generation microelectronics circuits will have minimum dimensions below 100 nm. It is envisioned that 157 nm laser lithography [27,28,28a] will be the next step in optical lithography. At 157 nm, under VUV illumination of the mask target, lithographic features with dimensions less than 0.10 μm on the photoresist could be achieved. However, there are problems related to the design of the optical projection system, due to the fact that the absorption coefficient of most materials in the VUV is large, yet, their optical properties degrade constantly with time under VUV irradiation. Up to now, only calcium fluoride seems to be promising as optical material for 157 nm photolithography, and the possibility of using wide band gap fluoride dielectric crystals, such as YF_4 and LiCaAlF_6 , as optical elements for 157 nm photolithography was investigated. These materials could be grown from melts at lower temperature than CaF_2 and they have similar physical properties, despite the fact that they are forming crystals of different symmetry than cubic. Doped or nondoped wide band gap crystals can be used as passive or active optical elements in the VUV: i.e., prisms, lenses, filters of variable and controllable attenuation [28, 28a].

All these applications depend on the development of new dielectric wide band gap materials, and the structure of the levels of the $4f^{n-1}5d$ electronic configuration that specify the d–f transitions of the RE ions. However, despite the early spectroscopic measurements of the f–d transitions [29], only limited information is available in this field. A small amount of data has been taken and analyzed with the use of VUV lasers, x-ray, or synchrotron light sources by exciting a common RE impurity in different dielectric fluoride crystal hosts. Investiga-

tion of fundamental physical interactions in the crystal environment is of considerable importance and will determine the response of these materials to VUV light.

II. VACUUM ULTRAVIOLET SPECTROSCOPY: METHODS AND TECHNIQUES

A. Molecular Fluorine Laser

Investigating physical processes in the VUV requires the use of intense sources of photons in this spectral range. For a detailed investigation of the absorption spectrum, the emission characteristics of the sources are such that either the radiation occurs as a continuum or the emission spectrum consists of closely packed lines. In addition, the continuous light sources should be stable with respect to time and the pulsed ones should have good pulse to pulse stability. In most experimental cases, the available continua source suitable for ultraviolet absorption studies is molecular hydrogen. Its molecular spectrum extending from the visible to 100 nm is obtainable from a low-pressure positive column discharge. Continua spectra have likewise been taken from positive column discharges in rare gases, from 60 to 200 nm. At higher pressures, the continuum in helium discharges could be extended up to 400 nm. Tunable VUV radiation can be generated from nonlinear methods using frequency mixing in rare gases and metal vapors [30–33] and nonlinear crystals [34,35]. However, the nonlinear methods are relatively complex and characterized by low conversion efficiency and low-output energy.

The major breakthrough in this direction was made in 1973 with the introduction of the excimer laser sources based on rare gas dimers. Strong dipole transitions between the bound electronic excited state and the dissociative ground state of diatomic clusters of Xe_2 , Kr_2 , and Ar_2 in liquid, gas, or solid phase [36–39] provided a new powerful radiation source in the VUV. These systems were characterized by high quantum efficiency in the emitted wavelength, high gain, and conversion efficiency. However, limited tunability and e-beam excitation to achieve population inversion imposes serious experimental restrictions on their use for spectroscopic applications.

At the present time, very few laser sources are available in the VUV (Table 1). Among them the ArF excimer laser with limited tunability at 193 nm [40,41], and the molecular fluorine laser at 157 nm [42–50], are the only efficient laser sources available on the laboratory scale. Laser transitions at 156.71, 157.48, and 157.59 nm have been observed for the first time by Woodworth and Rice [42,43] in F_2/He mixtures excited with an electron gun with high efficiency and in electric discharge-pumped lasers. The laser transition has been identified as of the ${}^3\Pi_{2g} \rightarrow {}^3\Pi_{2u}$ type and is the same as for the laser transition of the 301.5–346 nm band in molecular iodine. The energy difference between the first two transitions

Table 1 VUV Laser Sources

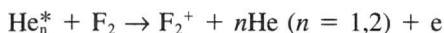
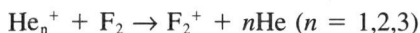
Laser	Emission wavelength (nm)	Excitation
H ₂	109.8–164.4	EB
D ₂	111.3–161.6	PD
Ar ₂	126	EB
Kr ₂	145.7	EB
F ₂	157.6	PD
ArCl	169, 175	PD
Xe ₂	170	EB
Kr ³⁺	175.6	CW
Cu	181	PD
Kr ⁴⁺	183.2	CW
Ar ⁴⁺	184.3	CW
CO	187.8, 189.7, 197	PD
ArF	193	PD
Kr ³⁺	195	CW
Kr ³⁺	196	CW

Population inversion is achieved commonly by electron beam (EB) or pulsed (PD) and continued (CW) plasma discharges.

was attributed to de-excitation from two different rotational levels of the same vibrational level of the $^3\Pi_{2g}$ state to the $^3\Pi_{2u}$, and the energy difference between the first and the third level to de-excitation from two different vibrational levels. The energy position of the $^3\Pi_u$ electronic state was found to be 3 eV above the $X^1\Sigma_g$ ground state from electron-scattering experiments [51]. This state is slightly bound by 0.15 eV [52].

The energy position of the lower vibrational level of the $^3\Pi_{2g}$ state was found to be 11.62 eV above the $X^1\Sigma_g$ ground state [53], which is in agreement with theoretical calculations [54].

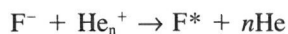
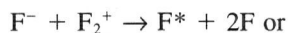
The kinetic scheme proposed [44] to explain the above transition in the plasma discharge assumes the production of metastable helium atoms He* and e⁻/He⁺ pairs. The He⁺ ions at high pressure are forming He₂⁺ and He₃⁺ ionized molecular clusters in the ground or excited states, which, finally, through effective collisions, either ionize the fluorine molecules or form atomic species:



Low-energy electrons can efficiently generate atomic fluorine negative ions



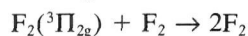
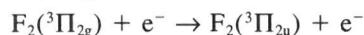
and then



The final result of the atomic and molecular collisions is the formation of the F_2 molecules in their excited $^3\Pi_{2g}$ electronic state:



Once the $\text{F}_2(^3\Pi_{2g})$ molecular species have been formed, they can be de-excited by spontaneous and stimulated emission and by collision quenching.



Electron excitation [42] is a relatively complicated method in comparison to the pulsed fast discharge, using LC-inversion or charge transfer circuits (Fig. 1) together with preionization of the gas mixture. Preionization is achieved by UV light, which is triggered a few nanoseconds before the main discharge [44,55,56]. As soon as the fast switch S (thyatron or spark-gap) closes (Fig. 1), the stored energy in the capacitor C_2 is transferred into the discharge volume through the capacitors C_1 . Double preionization (2×80 pins) of the laser volume ensures a uniform and stable main discharge. The electrodes were semicylindrical with round surfaces and no sharp edges, fabricated from stainless steel 316, 1 cm wide and 80 cm long, spaced 2 cm apart.

Good preionization in the circuit is essential to shape together with Rogowski profile electrodes, which are relatively difficult to machine in comparison to the semicylindrical profile. Stability of the discharge main mode was also ensured by the low inductance of the discharge circuit of 60 nH, which gives a fast rise

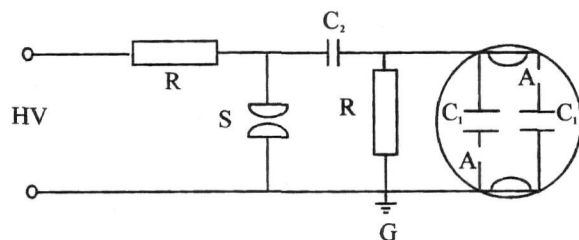


Figure 1 Schematic layout of the electric circuit of the ‘‘charge transfer type’’ F_2 laser. HV, high voltage; R, resistive load; S, spark gap; C_1 , C_2 , capacitors; A, preionization gap; G, ground.

time of the main charging voltage of 50 ns. The discharge volume is $100 \times 1.5 \times 0.3 \text{ cm}^3$, and this device can deliver 10 mJ at 157 nm per pulse at 2–3 atm total helium pressure. A typical pulse duration is of the order of 10–20 ns, and its spectral linewidth at FWHM is less than 0.05 nm [44]. The small signal gain coefficient of the previous pulsed discharge F_2 laser has been measured using the passive cell absorption method at 2 atm of the helium buffer gas. It was found to be $3.2\% \text{ cm}^{-1}$. This value was half that predicted by theory [47] considering only dissociative collision of the F_2 molecules by either ion–ion recombination or energy transfer reaction and neglecting direct excitation of the F_2 molecules by either electron impact or energy transfer from He^* and He_2^* molecules.

The small signal gain coefficient using the oscillator–amplifier method was found to be of the same order of magnitude and the saturation intensity was on the order of 4.5 MW/cm^2 [49,50]. Despite the fact that the value of the small signal gain coefficient at 157 nm is comparable to the value of the rare gas halide transitions of the excimer lasers up to 1988, the output energy at 157 nm never exceeded 15 mJ. This was mainly due to the presence of small amounts of organic impurities and air in the commercial gases and the experimental restrictions in raising the total gas pressure above 3 atm. The absorption coefficient of the air at 157 nm is higher than 200 cm^{-1} and therefore the net gain competed with the absorption losses. By increasing the pressure of the helium buffer gas to 8 atm, 112 mJ per pulse were obtained by Yamada et al. [48].

B. VUV Absorption Spectroscopy

Absorption cross-sectional investigations in the VUV require adequate measurement of the ratio of the incident to transmitted radiation. For atomic or molecular systems that exist in the gas state, accurate measurement of pressure and temperature is required. Measurement of the absorption coefficient of metal vapors is made even more difficult by the rapidity with which the reactive vapor attacks the windows of the absorption cell and by the high temperatures often necessary for the production of significant concentrations of the atoms.

For many experimental systems, measurement of the absorption coefficient is prohibited in the wavelength region below the cutoff wavelength of the LiF window (Fig. 2). For other experimental configurations, the source discharge gases are separated from the detector and the sample areas by differential pumping slits. In this case the cutoff wavelength is determined by the efficiency of the gas discharge and the cutoff wavelength of the monochromator and the photon detector (Fig. 3).

The absorption spectra of trivalent RE ions in the VUV in wide band gap dielectric crystals are due to the $4f^n \rightarrow 4f^{n-1}5d$ electronic transitions between the ground state of the $4f^n$ single electronic configuration and the Stark levels of the $4f^{n-1}5d$ mixed electronic configuration. Experimental apparatus for ob-

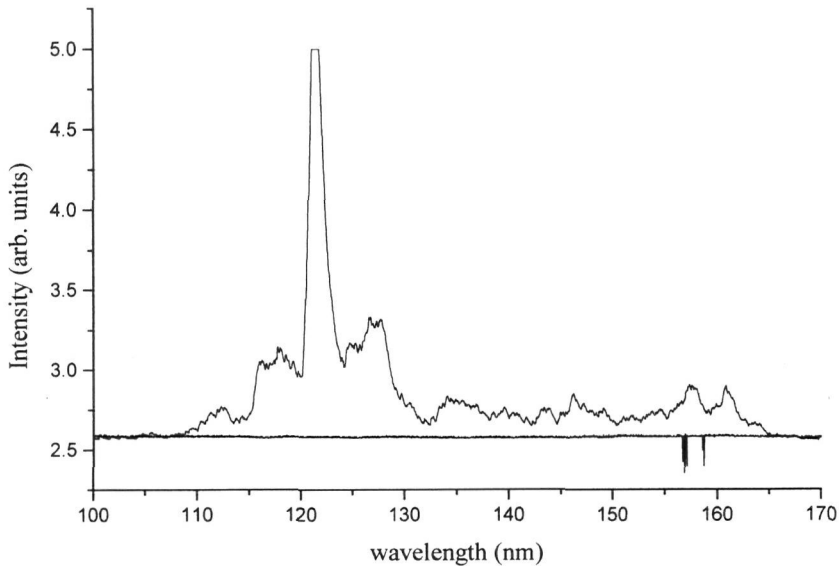


Figure 2 Emission spectrum from a longitudinal stabilized low-pressure hydrogen column recorded with a secondary electron multiplier (SEM), of open configuration. The hydrogen lamp was sealed with an LiF crystal window and it was the only optical element between the VUV lamp and the SEM. With this experimental configuration, the edge of the conduction band of wide band gap dielectric crystals can be determined accurately.

taining the absorption spectra consists mainly of a hydrogen VUV light source, the vacuum chamber where the crystal sample is placed, and the optical and electronic detection equipment (Fig. 4) [7]. The hydrogen light source operates in a longitudinally stabilized discharge mode. The discharge's high stability provides good signal-to-noise ratio (better than 2000). The optical paths of the light source and the fluorescence light beams are inside vacuum lines of stainless steel at 10^{-6} mbar pressure.

The vacuum chamber where the crystal samples are placed is equipped with a cryogenic facility. The optical detection system consists of a VUV monochromator, a solar blind photomultiplier, or a secondary electron multiplier (SEM). When a VUV photon is absorbed within the volume of the crystal sample, new VUV photons are re-emitted within the crystal at the same or different wavelength due to spontaneous emission from the levels of the $4f^N5d$ electronic configuration of the trivalent RE ions. The intensity of the radiation within the crystal volume V depends on the position of the atoms within the crystal and the wavelength [57].

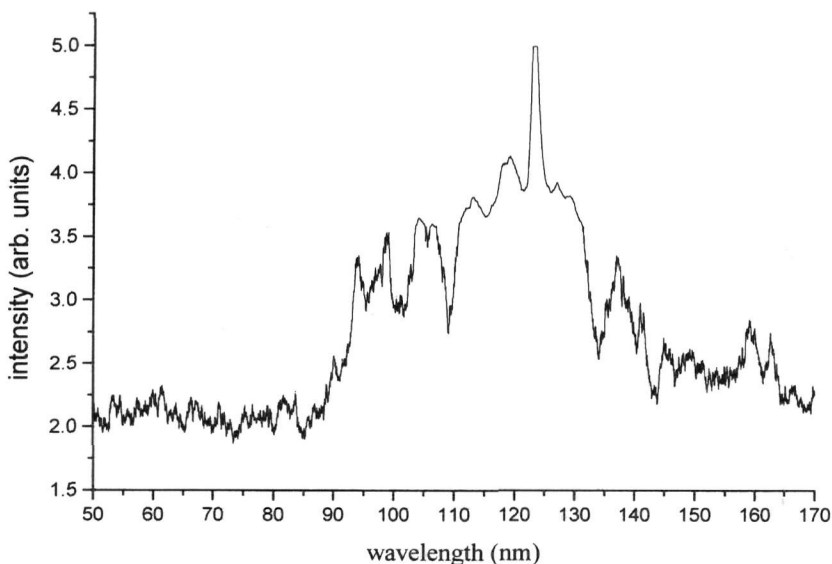


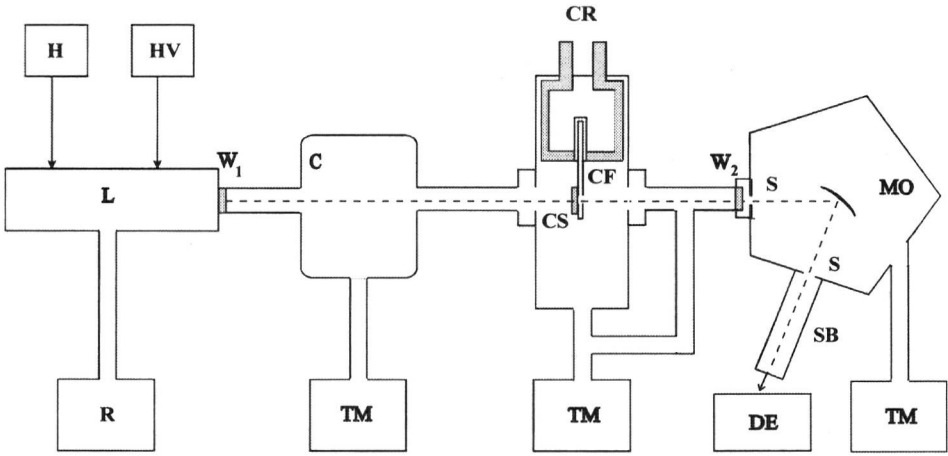
Figure 3 Emission spectrum from a longitudinal stabilized hydrogen lamp. No optical element was placed between the hydrogen discharge column and the secondary electron multiplier (SEM). The hydrogen flow through the discharge cell was controlled with differential pumping at different stages between the discharge and the SEM.

$$\frac{\partial I(\lambda, x)}{\partial x} = [N_2 - N_1]F(\lambda) \left(\frac{Bh\lambda}{Vnc^2} \right) I(\lambda, x) \quad (1)$$

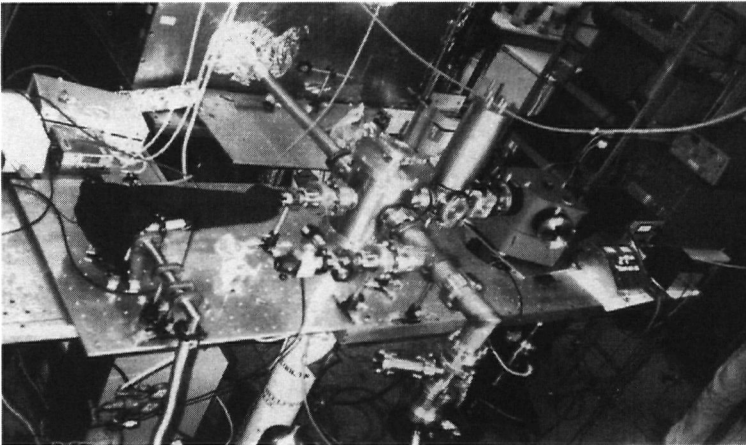
where N_2 and N_1 are the excited and the ground state populations of the atomic transition at λ , $F(\lambda)d\lambda$ is the fraction of the transitions in which the photon frequency lies in a small range $d\lambda$ about the wavelength λ , V is the total crystal volume where the interaction of radiation with matter occurs, B is Einstein's coefficient, and n is the refractive index of the crystal. The solution of this equation is more complicated than it first appears because N_2 and N_1 themselves depend on the intensity of the radiation and hence on the position of the atoms inside the crystal and the wavelength of light. Eq. (1) takes the form

$$\frac{\partial I(\lambda, x)}{\partial x} = [a(\lambda, x) - \beta(\lambda, x)]I(\lambda, x) \quad (2)$$

where $a(\lambda, x)$ is the gain coefficient that describes photon generation through spontaneous emission and $\beta(\lambda, x)$ is the absorption coefficient.



(a)



(b)

Figure 4 a. Schematic layout of the VUV absorption spectrometer. H, hydrogen supply; HV, high voltage; L, longitudinal stabilized hydrogen discharge $W_{1,2}$, LiF windows; C, vacuum chamber; CF, cold finger; CS, crystal sample; CR, cryostat; MO, VUV monochromator; S, slits; TM, turbo molecular pump; DE, detection electronics; SB, photomultiplier or secondary electron multiplier. b. X-UV and VUV absorption spectrometer at the National Hellenic Research Foundation (Athens, Greece). Crystal samples could be cooled down to 10K with a closed circle helium cryostat. Further cooling to 4.2 K can be achieved with a specially constructed liquid helium cryostat.

The solution of Eq. (2) is

$$I(\lambda, x) = I(\lambda, x = 0) e^{\int_0^x [a(\lambda, x) - \beta(\lambda, x)] dx} \quad (3)$$

Taking into consideration that the gain coefficient $a(\lambda, x)$ is proportional to the number density of the excited atoms $N_2(x)$ and thus proportional to the intensity of light

$$a(\lambda, x) = \sigma(\lambda)N_2(\lambda, x) \quad N_2(\lambda, x) = cI(\lambda, x) \quad (4)$$

Equation (3) then becomes

$$I(\lambda, x) = I(\lambda, x = 0) \exp \left\{ \int_0^x [\sigma(\lambda)cI(\lambda, x) - \beta(\lambda, x)] dx \right\} \quad (5)$$

This equation can be solved using successive iterations. As zero order approximation we consider the case where there is no secondary photon generation and the absorption coefficient is independent on the position of the interacting atoms inside the crystal. In this case the solution of the equation takes its usual form (Lambert–Beer law)

$$I^{(0)}(\lambda, x) = I(\lambda, x = 0) \exp \left[\int_0^x -\beta(\lambda, x) dx \right] \quad (6)$$

Substituting Eq. (6) into Eq (3) we get $I^{(1)}(\lambda, x)$ in first-order approximation.

$$I^{(1)}(\lambda, x) = I(\lambda, x = 0) \exp \left\{ \int_0^x [\sigma(\lambda)cI(\lambda, x' = 0) e^{-\beta(\lambda)x'} - \beta(\lambda)] dx \right\} \quad (7)$$

Integrating the above equation and setting

$$F^{(1)}(\lambda, x) = \exp \left[c\sigma(\lambda) \frac{I(\lambda, x = 0)}{\beta(\lambda)} (1 - e^{-\beta(\lambda)x}) \right] \quad (8)$$

Equation (7) becomes

$$I^{(1)}(\lambda, x) = I(\lambda, x = 0) F^{(1)}(\lambda, x) e^{-\beta(\lambda)x} \quad (9)$$

The $F^{(1)}(\lambda, x)$ term that describes deviation of the absorption processes from the law of Lambert and Beer is a function of wavelength and the crystal thickness. It describes photon emission through spontaneous emission within the crystal volume in first-order approximation. By measuring the photon intensity emitted from the crystal $I^{(1)}(I, x)$ as a function of the crystal thickness, the $F^{(1)}(\lambda, x)$, can be determined.

In the case of “optically thin” samples, $\beta x \ll 1$, Eq. (9) takes the form

$$I^{(1)}(\lambda, x) \approx I(\lambda, x = 0) \exp(ax) \approx I(\lambda, x = 0)(1 + ax) \quad (10)$$

Under these experimental conditions, the emitted photon intensity from the crystal is taking place through spontaneous emission processes and varies linearly with crystal thickness. Similarly when $\beta x \gg 1$, “optically thick sample” Eq. (9) takes the form

$$I^{(1)}(\lambda, x) \approx I(\lambda, x = 0) e^{[\alpha(\lambda)/\beta(\lambda)]} \approx I(\lambda, x = 0) \left[1 + \frac{a(\lambda)}{\beta(\lambda)} + O\left(\frac{a(\lambda)}{\beta(\lambda)}\right) \right] \quad (11)$$

In this case the emitted intensity from the crystal is independent on its thickness. For cases between Eqs. (10) and (11), the emission is reduced by self-absorption and care has to be taken to ensure that all the terms in the transfer equation are properly allowed for individual cases. When a single RE ion absorbs one VUV photon, the $4f^{n-1}5d$ electronic configuration is populated and competition starts between radiative and nonradiative transitions. The excited ion decays to the different levels of the $4f^{n-1}5d$ electronic configuration and subsequently relaxes to the ground level of the $4f^n$ electronic configuration with VUV or UV photon emission. It is therefore expected that the $F^{(1)}(\lambda, x)$ factor will be equal to unity for the spectral region where there is no photon emission. In this case, absorption processes inside the crystal sample fall within the validity of the Lambert and Beer’s law [Eq. (9)]. For example, in the case of the $\text{LiYF}_4:\text{Nd}^{3+}$ crystal, spontaneous emission modulates the value of the absorption coefficient only in the spectral range from 180 to 182 nm, since the crystal emits strongly in this spectral range when it is excited with VUV laser light at 157 nm [7].

III. OPTICAL AND ELECTRONIC PROPERTIES OF WIDE BAND GAP FLUORIDE DIELECTRIC CRYSTALS DOPED WITH TRIVALENT RE IONS

A. Electronic Properties of Wide Band Gap Materials

The optical properties of the nondoped wide band gap dielectric crystals in the VUV are mainly due to transitions from electronic states between the valance and the conduction band. The high value of the absorption coefficient, for photon energies higher than the crystal’s band gap, is due to transitions involving delocalized electronic states in the conduction band, and arise from the crystal symmetry. The crystals’ energy bands are formed from the energy levels of atoms when they are brought close together. On the other hand, local lattice imperfections, vacancies and other point defects, and dislocations bring about the formation of allowed states connected with the perturbation area. The electronic wavefunctions of such states are nonzero in approximately the same area where the perturbation exists. In other words, the electron is localized in the perturbation area. The smaller the perturbation energy, the greater the localization area. In this case,

transitions are taking place between the valance band and the localized states in the conduction band. The width of the band gap is proportional to the value of the exchange integral, the origin of which is the fact that the electrons may, with some probability, be located near any atom. The exchange integral can be calculated with perturbation theory and accepting electron states of an isolated atom as zero approximation for the solution of the Schrödinger equation for the electron in a periodic crystal field $U(r)$.

$$\begin{aligned}\hat{H}\Psi(r) &= E\Psi(r) \\ \hat{H} &= -\frac{\hbar^2}{2m}\Delta + U(r); U(r) = U(r + n)\end{aligned}\quad (12)$$

denoting the Hamiltonian of an isolated atom by

$$\begin{aligned}\hat{H}_a &= -\frac{\hbar^2}{2m}\Delta + V_a(r) \\ \hat{H}_a\Psi_a(r) &= E_a\Psi_a(r)\end{aligned}\quad (13)$$

where $V_a(r)$ is the potential energy of the electron in an isolated atom, E_a is the a energy level, and $\Psi_a(r)$ is the wavefunction corresponding to E_a . Solution of the equation for the atom is supposed to be known. The zero-order electron wavefunction in the crystal $\Psi^{(0)}(r)$ should be the sum of the atomic wavefunctions at the point $r - m$ that satisfy the translational condition at the point $r \pm m$, and n is the coordinate of an ion.

$$\Psi^{(0)}(r) = \sum_m \exp(ikm)\Psi_a(r - m) \quad (14)$$

Zero approximation of the wavefunction $\Psi^{(0)}(r)$ enables the first approximation for the energy of the electron in the crystal field $E^{(1)}$ to be calculated

$$E^{(1)} = \frac{N \left[E_a \sum_p \exp(ikp)S_p + C + \sum_p \exp(ikp)A(p) \right]}{N \sum \exp(ikp)S_p} \quad (15)$$

where S_p is the overlapping integral that depends not on the coordinates of two ions, but also on the distance p between them

$$\int \Psi_a(r')\Psi_a(r' - p) = S_p \quad (16)$$

and $A(p)$ is the exchange energy

$$A(p) = \int \Psi_a^*(r') \left[\sum_{n \neq p} V_a(r' - n) + W(r') \right] \Psi_a(r' - p) d\tau' \quad (17)$$

where $W(r')$ is the periodic self-consistent lattice field

$$W(r) = U(r) - \sum_n V_a(r - n) \quad (18)$$

$A(p)$ is made up of the wave functions of two atoms separated by the distance p , with the physical meaning that the two atoms at distance p from each other may exchange electrons. The exchange proceeds through the field of all other atoms and the periodic self-consistent part of the lattice field $W(r)$. Due to the exponential form of the atomic wavefunctions, the exchange takes place mainly between neighboring atoms. Electron exchange between any two atoms of the crystal takes place by way of chain of neighbor exchanges. Therefore, electrons are not localized near individual atoms but move freely through the crystal jumping from one atom to another by the exchange process. From Eq. (15), the energy of the atomic electrons in a crystal field is revealed. When the interaction of the electrons with the ions and with the other electrons is taken into account, the energy levels are lowered by the amount C and split into a band of definite width. Because $S_p \approx 0$ when $p \neq 0$, we may write

$$E^{(1)} = E_a + C + \sum_p \exp(ikp)A_p \quad (19)$$

For a simple cubic lattice like the LiF crystal, every atom has six nearest neighbors with the coordinates $\alpha[(1,0,0), (-1,0,0), (0,1,0), (0,-1,0), (0,0,1), (0,0,-1)]$. Assuming exchange energy to be isotropic and neglecting electron exchange between distant atoms we obtain

$$E^{(1)} = E_a + C + 2A(\cos k_x a + \cos k_y a + \cos k_z a) \quad (20)$$

The energy depends quascontinuously on the wave vector k and changes from E_{\min} to E_{\max}

$$\begin{aligned} E_{\min} &= E_a + C + 6A \\ E_{\max} &= E_a + C - 6A \end{aligned} \quad (21)$$

Thus, as a result of the atomic interaction, the energy level of an isolated atom in a cubic crystal lattice drops by the amount C and splits into a band $12A$ wide. The energy band gap depends on the exchange energy A . But the exchange energy itself is dependent on the area of the overlapping of the wave functions: the more the atomic wave functions overlap, the greater will the ex-

change energy be. It follows from here that energy levels corresponding to inner shell electrons do not split as intensely as those of the outer shells, since the inner shell electrons are localized in smaller areas of space. As the energy increases, bands become wider and the gaps narrower. The higher a level, the lower it drops and the wider it spreads. This result is basic for explaining the dependence of the band gap width on the atomic number of the elements belonging to the same group. For example the width of the forbidden band between the valance and the conduction band for the metals Li, Na, K, Sc, and the halogens F, Cl, Br I should decrease in the same order.

Following the above arguments it is expected that the LiF crystal will have the widest band gap, among all the dielectric crystals, a fact that is verified from experiments. Optical transitions in the VUV might take place between the valance and the core band of the metal cations, which are formed of electron orbitals lying lower in energy than the ones forming the valance band ($2p F^-$). In this case an electron is excited from the core band to the conduction band. The hole created in the core band relaxes very fast to the band edge and is subsequently annihilated by electron capture from the filled valance band.

The conservation of energy in this case requires emission of a VUV or UV photon. The process is known as cross-relaxation [58] and it has been observed in different wide band gap dielectric crystals [59]. Band-to-band excitonic transitions in the VUV have been observed in various wide band gap materials such as LiCaAlF_6 [60] and LiYF_4 [61] crystals doped with Nd^{3+} and Ho^{3+} ions, respectively. In these cases, the peaks around 114, 118, and 112, 116, 119 nm might correspond to excitonic transitions between the valance and the conduction band of the host lattice. The excitonic transitions imply a large value of the index of refraction of fluoride crystals in the VUV, in agreement with previous measurements [62–70].

Considering that the cut-off wavelength of the LiF window (which is placed in front of the hydrogen lamp and the solar blind photomultiplier) is at 110 nm (for commercial LiF windows 5 mm thick) (Fig 2.), the absorption spectrum between 113 and 120 nm indicates only the energy of the corresponding transitions. The edge of the conduction band is extended over a relatively wide spectral range (113–120 nm). This situation reflects that the electron wavefunctions of the fluorine and the metal ligands are extended over a large range as is expected from the strong electrostatic nature of the corresponding bonds. The main contribution at the value of the absorption coefficient in the spectral range from 110 to 120 nm is from the absorption of light within the conduction band of the LiCaAlF_6 crystal. The absorption within the conduction band of the LiCaAlF_6 crystals is at least one order of magnitude higher than the absorption within the $4f^2 5d$ electronic configuration. As a consequence of the large value of the absorption coefficient in this spectral region, it falls out of the dynamic range of the absorption spectrometer and hence deviates significantly from its mean value. Optical transitions in the VUV are likewise taking place between the valance

and charge transfer bands situated inside the band gap of the host crystal. They are formed by strong electrostatic interactions between the d electron of the trivalent RE ions and the anions of the host crystal [71–74].

IV. VUV ABSORPTION SPECTROSCOPY OF TRIVALENT RE IONS IN WIDE BAND GAP FLUORIDE CRYSTALS

When a particular atom or ion is surrounded by a symmetrical distribution of atoms or ions (ligands), many new properties emerge that were not present in the free atom case. There are two models for the treatment of such systems. In the first model the central atom is assumed to be surrounded by a distribution of charges that produces an electrostatic field at the position of the central atom. In this model (*crystal field*) there is no sharing of electronic charge between the central atom and the ligands. The second model treats the central atom and its ligands as if they were a single molecule (*molecular-orbital method*). In this case electrons are permitted to overlap. In most cases this model is treated by the methods of molecular-orbital theory. In both cases symmetry considerations are of great importance. The symmetry of the optical site determines the degeneracy of the electronic states and the optical properties of the materials. In the case of wide-band-gap dielectric crystals doped with trivalent RE ions, the crystal field model is usually applied since it is simpler, and the optical properties of the RE ions are determined by the influence of the crystal field on the Hamiltonian of the free ion.

In order to assign the dipole-allowed transitions between the Stark components of the $4f^{n-1}5d$ electronic configuration and the levels of the $4f^n$ electronic configuration, the exact solution of the secular equation of the $4f^{n-1}5d$ electronic configuration in the presence of the crystal field should be known [75,76]. However up to now, there have been no detailed theoretical calculations of the energy position of the levels of the $4f^{n-1}5d$ electronic configuration. Crystal field calculations are carried out only to a low order of perturbation theory where the strongest perturbation is applied first, followed by the next strongest, etc. [77]. The exact theoretical treatment of the energy level problem of the $4f^{n-1}5d$ electronic configuration is difficult to address. Even for the simplest case of the Ce^{3+} ion, the crystal field for a d electron in a cubic symmetry requires 10 parameters for its characterization. In order to identify these from the experimental data, one must resolve and identify at least 11 spectral lines within the configuration. The number of lines within the configuration is large (20 for Pr^{3+} , 3106 for Tb^{3+} ions) and as a consequence attempts to evaluate crystal-field parameters by fitting an experiment are difficult.

In principle, if one knows the radial wave functions of the ion in question, then the crystal field perturbation can be calculated and the energy levels can be compared with the experimental values. However, it is tedious to construct

wavefunctions of the electrons in the $4f^{n-1}5d$ mixed configurations, and only qualitative interpretation of the absorption spectra has been available up to now. The early attempt of Dieke [29] to deduce the extent of the $4f^{n-1}5d$ electronic configuration for each of the RE ions was made using experimental data and some observed regularities in the lanthanide spectra. The effect of the crystal field on the $4f^{n-1}5d$ electronic configuration is to lower its energy in comparison to the free ion case (Table 2).

Various empirical methods have been developed [77] to interpret the VUV absorption spectra of the $4f^{n-1}5d$ electronic configuration. These are based on the following principle. The energy difference Δ between two configurations differing by a single electron in the 4f configuration (e.g., $4f^n$ and $4f^{n-1}5d$) is constant for all the lanthanides. This allows the evaluation of the energies of different configurations for free ions with different ionization. Brewer [77] used this to estimate the energy of the lowest energy level of a given configuration, beginning with measured energies for neutral rare earths. For the 5d electronic configuration of the RE ions, the crystal field perturbation is stronger than the electron–electron interaction, due to the fact that the d electron is extended over a large distance and been far apart from the nucleus of the ion. In this case the effect of the crystal field is calculated first or simultaneously with the imposition of the Coulomb interaction followed by the spin–orbit interaction. For example for the D_4 tetragonal symmetry, the energy levels are the following: $\Gamma^{(4)}$, $\Gamma^{(5)}$, $\Gamma^{(3)}$, and $\Gamma^{(1)}$.

When the spin and the spatial parts of the wave functions are coupled within the framework of the symmetry group of the RE ion, the number of the energy levels is described by the decomposition of the product representation of $\Gamma^{(6)}$ (spin part) with $\Gamma^{(4)}$, $\Gamma^{(5)}$, $\Gamma^{(3)}$, and $\Gamma^{(1)}$. The new energy levels now are the following: $\Gamma^{(7)}$ (2B_2), $\Gamma^{(6)}$ (2E), $\Gamma^{(7)}$ (2E), $\Gamma^{(7)}$ (2B_1), $\Gamma^{(6)}$ (2A_1). In addition, when only one electron is present in the 5d orbital, as concerns the symmetry of the states produced by the combined action of the crystal field and the spin–orbit interaction, it makes no difference in which order the two perturbations are applied. The symmetry group of the atom is no longer the three-dimensional rotation group because all directions in space are no longer equivalent. Instead, the symmetry is that of a point group containing a finite number of elements and is a subgroup of the three-dimensional rotation group. An irreducible representation of the latter becomes reducible with respect to the lower symmetry point group. The spherical harmonics are not any longer energy eigenstates and are transformed under the irreducible representations of the symmetry operators of the three-dimensional rotation group to its linear combinations. The effect on the states of the free atom is to remove degeneracy. The first-order energies are sensitive to the magnitude of the interactions and hence to the order in which they are applied.

In the case where the Coulomb repulsion of the electrons or the spin–orbit interaction is the strongest perturbation, as in the case of the $4f^n$ or the $4f^{n-1}$ electronic configuration [78], which are well shielded by the 6p and the 6s elec-

Table 2 Energy Position of the Edge of Levels of $4f^{n-1}5d$ Electronic Configuration of Trivalent RE Ions

RE ³⁺ ion	Free RE ³⁺ ions $\times 10^3$ cm ⁻¹	YF ₃ \times 10 ³ cm ⁻¹	LuF ₃ \times 10 ³ cm ⁻¹	LiYF ₄ \times 10 ³ cm ⁻¹	LaF ₃ \times 10 ³ cm ⁻¹	BaY ₂ F ₈ \times 10 ³ cm ⁻¹	CaF ₂ \times 10 ³ cm ⁻¹	KY ₃ F ₁₀ \times 10 ³ cm ⁻¹
Nd ³⁺	70.1	58.4	57.1	54.6	60.0	53.3		53.8
Er ³⁺	75.4	64.3	63.8	62.5	64.7	61.9		63.3
Tm ³⁺	74.3	63.4	63.0	61.5	64.4		63.0	
Ce ³⁺	49.7			34.4	38.8	34.0	31.9	
Ho ³⁺	58.9			63.3	63.3	63.1	64.1	

Values are given as measured from the ground level of the $4f^n$ electronic configuration in different crystal hosts.

tronic configurations, the transformation properties of the electronic wavefunctions are well described by the three-dimensional rotation group $O^+(3)$ and the spherical harmonics are basic functions for the representations $D^{(l)}(\alpha, \beta, \gamma)$ of the $O^+(3)$. The subsequent application of the crystal field will further split the energy levels.

Vacuum absorption and emission spectra of the trivalent RE ions in wide band gap fluoride crystals are due to the interconfigurational $4f^{n-1}5d \leftrightarrow 4f^n$ transitions of the RE ions. They have been interpreted by fitting the crystal field splitting of the d electronic configuration to the energy gaps in the ground multiplets of the $4f^{n-1}$ core [79]. The high complexity of the energy level systems of the trivalent RE ions in the $4f^{n-1}5d$ electronic configuration makes a detailed interpretation of the observed spectra still impossible. This is mainly due to the fact that the wave functions of the two electronic configurations are transformed differently under the symmetry operations and the classification of spectral terms is rather difficult, since the selection rules for the angular momentum are no longer valid.

A theoretical interpretation of the atomic spectra of the $4f^{n-1}5d$ electronic configuration was based on the finding, that the interaction energy of the crystal field with the d electron exceeds the Coulomb interaction energy between the d and the $4f^{n-1}$ electrons [80]. Energy states of the d electron are characterized by irreducible representations of the corresponding crystal symmetry group $\Gamma^{(2)}$. For the $4f^{n-1}$ electronic configuration, L–S coupling is predominant and further splitting of energy levels is taking place (Table 3). The energy levels are characterized by the $\Gamma^{(1)}$ index of the irreducible representation of the three-dimensional rotation group.

For this method the electronic wave functions can be written in the form $|\text{SLJ}\Gamma^{(1)}, \Gamma^{(2)}, \alpha\Gamma\mu\rangle$, where μ is the number of the basis function of the irreducible representation Γ , and the index α identifies the representation Γ that appears several times in the direct product representation $\Gamma^{(1)} \times \Gamma^{(2)}$.

A qualitative interpretation of the $4f^{n-1}5d \leftrightarrow 4f^n$ interconfigurational transitions of trivalent RE ions in wide band gap dielectric crystals was made by Szczurek and Schlesinger [81]. They constructed spectral terms first (the selection rules for angular momentum are valid in this case), and then allowed for crystal field splitting. Because the electronic wave functions of the $4f^{n-1}$ and 5d electronic configurations have different transformation properties, this approximation is expected to be valid for the situation in which a more or less uniform charge distribution of the ligands takes place within the unit crystal cell. This is possible provided that the radius of the d orbital is smaller than lattice constants. In this case, the electric field around the origin for a given distribution of ligands is more or less spherical. This situation partially restores the three-dimensional rotation symmetry of the 5d electronic configuration. As a first approximation, the 5d and $4f^{n-1}$ electronic configurations might well have the same transformation properties under the three-dimensional rotational group.

Table 3 Crystal Field Splitting of the Main Levels of the $4f^2$ Electronic Configuration in the Presence of Crystal Field with Octahedral (O) and Tetragonal (D_4) Symmetry

Configuration	Terms	Levels	O	D_4
f^2	1S	1S_0	$^1\Gamma_1$	$^1\Gamma_1$
	3P	3P_2	$^3\Gamma_3 + ^3\Gamma_5$	$^1\Gamma_1 + ^1\Gamma_3 + ^1\Gamma_4 + ^1\Gamma_5$
		3P_1	$^3\Gamma_4$	$^1\Gamma_2 + ^1\Gamma_5$
		3P_0	$^3\Gamma_1$	$^3\Gamma_1$
	1I	1I_6	$^1\Gamma_1 + ^1\Gamma_2 + ^1\Gamma_3 + ^1\Gamma_4 + 2^1\Gamma_5$	$2^1\Gamma_1 + ^1\Gamma_2 + 2^1\Gamma_3 + 2^1\Gamma_4 + 3^1\Gamma_5$
	1D	1D_2	$^1\Gamma_3 + ^1\Gamma_5$	$^1\Gamma_1 + ^1\Gamma_3 + ^1\Gamma_4 + ^1\Gamma_5$
	1G	1G_4	$^1\Gamma_1 + ^1\Gamma_3 + ^1\Gamma_4 + ^1\Gamma_5$	$2^1\Gamma_1 + ^1\Gamma_2 + ^1\Gamma_3 + ^1\Gamma_4 + 2^1\Gamma_5$
	3F	3F_4	$^3\Gamma_1 + ^3\Gamma_3 + ^3\Gamma_4 + ^3\Gamma_5$	$2^3\Gamma_1 + ^3\Gamma_2 + ^3\Gamma_3 + ^3\Gamma_4 + 2^3\Gamma_5$
		3F_3	$^3\Gamma_2 + ^3\Gamma_4 + ^3\Gamma_5$	$3^3\Gamma_2 + ^3\Gamma_3 + ^3\Gamma_4 + 2^3\Gamma_5$
		3F_2	$^3\Gamma_2 + ^3\Gamma_3$	$3^3\Gamma_1 + ^3\Gamma_3 + ^3\Gamma_4 + ^3\Gamma_5$
	3H	3H_6	$^3\Gamma_1 + ^3\Gamma_2 + ^3\Gamma_3 + ^3\Gamma_4 + 2^3\Gamma_5$	$2^3\Gamma_1 + ^3\Gamma_2 + 2^3\Gamma_3 + 2^3\Gamma_4 + 3^3\Gamma_5$
		3H_5	$^3\Gamma_3 + 2^3\Gamma_4 + ^3\Gamma_5$	$3^3\Gamma_1 + 2^3\Gamma_2 + ^3\Gamma_3 + ^3\Gamma_4 + 3^3\Gamma_5$
		3H_4	$^3\Gamma_1 + ^3\Gamma_3 + ^3\Gamma_4 + ^3\Gamma_5$	$2^3\Gamma_1 + ^3\Gamma_2 + ^3\Gamma_3 + ^3\Gamma_4 + 2^3\Gamma_5$

A uniform charge distribution could be the result of charge compensation from the F^- ligands, or of the localized character of the d orbitals. For example, for a hydrogen-like atom, the expectation value of the radius of the electronic cloud $\langle r \rangle$ is given by the formula

$$\langle r \rangle = \frac{\alpha_0}{2Z} [3n^2 - l(l + 1)] \tag{22}$$

where n is the principal quantum number equal to 5, α_0 is the Bohr radius of the atom, $\alpha_0 = 0.053$ nm, Z is the charge of the nucleus, and $l = 2$. For Nd^{3+} , Tb^{3+} , and Ho^{3+} ions, the calculated values of the ionic radii are $\langle r \rangle \sim 0.028, 0.027,$ and 0.030 nm. The experimentally measured values for the three trivalent ions in CaF_2 are 0.11, 0.10, and 0.97 nm. Since the ionic radii of the F^- ions are 0.136 nm, and taking into consideration that the distance between two neighboring atoms is of the order of ~ 0.5 nm (as in $LiYF_4$ crystal), the spherical symmetry is expected to be restored partially by charge compensation from F^- ions and the localized character of the d orbital. Using this approximation, the number of experimentally observed transitions is in excellent agreement with the number

of theoretically expected $4f^n \rightarrow 4f^{n-1} 5d$ dipole-allowed transitions for Nd^{3+} and Tb^{3+} ions [82,83]. (See Table 4.)

A. Cerium (Ce^{3+} , $4f^1$)

The Ce^{3+} ion has only one electron in the d electronic configuration and therefore the spectroscopic assignment of the energy levels is simple. The free Ce^{3+} ion in the 4f electronic configuration has two energy levels— $^2F_{5/2}$, $^2F_{7/2}$,—which are separated by 2253 cm^{-1} . In the d electronic configuration it has also two levels— $^2D_{3/2}$, $^2D_{5/2}$ —which are separated by $49,733$ and $52,226 \text{ cm}^{-1}$ from the ground state, respectively. The crystal field splitting of the energy levels of the 5d electronic configuration depends on the site symmetry of the Ce^{3+} ions. The fivefold degenerate d level split into two levels with degeneracies 2 and 3. The d orbitals (z^2 , $d_{x^2 - y^2}$, d_{yz} , d_{zx} , and d_{xy}) are the basis functions for the $D^{(2)}$ representations of $O^+(3)$ group and the reduction of the $D^{(2)}$ into irreducible representations of the cubic group is $E(\Gamma^{(3)}) + T_2(\Gamma^{(5)})$. Since E and T_2 are two- and three-dimensional respectively, the energy levels associated with E and T_2 are doubly and triply degenerate. When the site symmetry of the Ce^{3+} ion is further reduced to a tetragonal D_4 one, degeneracy of the energy levels is removed since the irreducible representations of the cubic group are reducible representations of the D_4 group. The energy levels are split further and the degeneracy is removed: $E(\Gamma^{(3)}) = ^2A_1(\Gamma^{(1)}) + ^2B_1(\Gamma^{(3)})$, $T_2(\Gamma^{(5)}) = ^2A_1(\Gamma^{(1)}) + ^2B_1(\Gamma^{(3)})$. The absorption spectra of the Ce^{3+} ions in dielectric crystal hosts are attributed to the dipole-allowed transitions between the $^2F_{5/2}$ ground state of the 4f electronic configuration and the energy levels of the 5d electronic configuration observed early mainly due to experimental reasons, since the Ce^{3+} ions absorb and emit in the UV [84–99]. Six strong interconfigurational dipole-allowed transitions have been observed [92,96]. Four transitions have been assigned to the interconfigurational $4f \rightarrow 5d$ electronic transitions of the Ce^{3+} ions of tetragonal site symmetry, and two to clusters formed by two or more Ce^{3+} ions. One more transition of low intensity corresponds to the e_g level, which is doubly degenerate [97]. The remaining e_g level indicates a strong localized vibrational structure [81]. In this case the electronic wavefunctions of the Ce^{3+} ions do not overlap with the wavefunctions of the ions of the host lattice [99] and the strongest phonon lines are those corresponding to localized phonon frequencies.

B. Praseodymium (Pr^{3+} , $4f^2$)

Energy levels of the free Pr^{3+} ion in various electronic configurations such as $4f^2$, $4f5d$, $4f6s$, and $4f6p$ have been analyzed by Sugar [100]. A comparison of all the third and the fourth spectra of the lanthanide ions show a similarity

throughout the series [101]. Energy levels of the $4f^2$ electronic configurations have been identified by comparing spectra in the vapor phase and in $\text{LaCl}_3:\text{Pr}^{3+}$ crystals [102]. The lines arising from the $4f^2 \rightarrow 4f5d$ transitions were identified in a series of exposures of sparks made with successively increasing current. The energy levels were assigned by comparing the level structure with that of the isoelectronic Ce^{2+} ion and from relative line intensities [103]. The free Pr^{3+} ion in the $4f5d$ electronic configuration has 18 energy levels, the lowest is the 1G_4 at $61,171 \text{ cm}^{-1}$. The $^3G_{3,4,5}$, $^3H_{4,5}$ levels are excited through dipole-allowed transitions from the 3H_4 ground state of the $4f^2$ electronic configuration. The absorption spectra of the $4f^2$ and the $4f5d$ electronic configurations of the Pr^{3+} ions were studied previously in a number of crystal lattices [8,104–110]. If the Pr^{3+} ion is located at a C_{4v} symmetry center, the $^3G_{3,4,5}$ and the $^3H_{4,5}$ energy levels are split for a total number of 35 Stark levels [81].

The number of absorption lines in $\text{CaF}_2:\text{Pr}^{3+}$ crystals is about half that, but some lines may be weak or superimposed on others. If only the strongest lines are considered, an additional selection rule $\Delta J = \Delta L$ is applied in the C_{4v} symmetry, the number of Stark levels is limited to 12, which is close to what was experimentally observed [81]. In the case of a high concentration of the Pr^{3+} ions (higher than 0.01 at.%), the appearance of additional lines in the absorption spectrum is attributed to Pr^{3+} clusters and sites of additional symmetries. A typical VUV absorption spectrum for the $\text{KY}_3\text{F}_{10}:\text{Pr}^{3+}$ crystal for 0.1 at.% concentration of the Pr^{3+} ions at room temperature is indicated in Figure 5.

The $4f5d$ electronic configuration in the free ion case is extended between $61,170$ and $78,776 \text{ cm}^{-1}$. The edge of the levels of the $4f5d$ electronic configuration in various fluoride dielectric crystals is extended down to $44,440 \text{ cm}^{-1}$ and depends on the host material. For example, the edge of the levels of the $4f5d$ electronic configuration in LiLuF_4 crystal hosts is at $45,100 \text{ cm}^{-1}$ [8], in CaF_2 at $45,450 \text{ cm}^{-1}$ [81], and in LaF_3 at $49,995 \text{ cm}^{-1}$ [110]. The $4f^2$ electronic configuration of the Pr^{3+} ions consists of 13 energy levels. 1S_0 is the highest one, which lies very close to the $4f5d$ electronic configuration. The energy position of the 1S_0 level is within the $4f5d$ electronic configuration for most of the cases. For the LaF_3 crystal, the 1S_0 level is situated 3000 cm^{-1} below the edge of the band [111], and hence it can be highly populated from the $4f5d$ electronic configuration. A similar position of the 1S_0 energy level is valid for the YF_3 [24] and most of the oxide crystal hosts [112–114].

C. Neodymium (Nd^{3+} , $4f^3$)

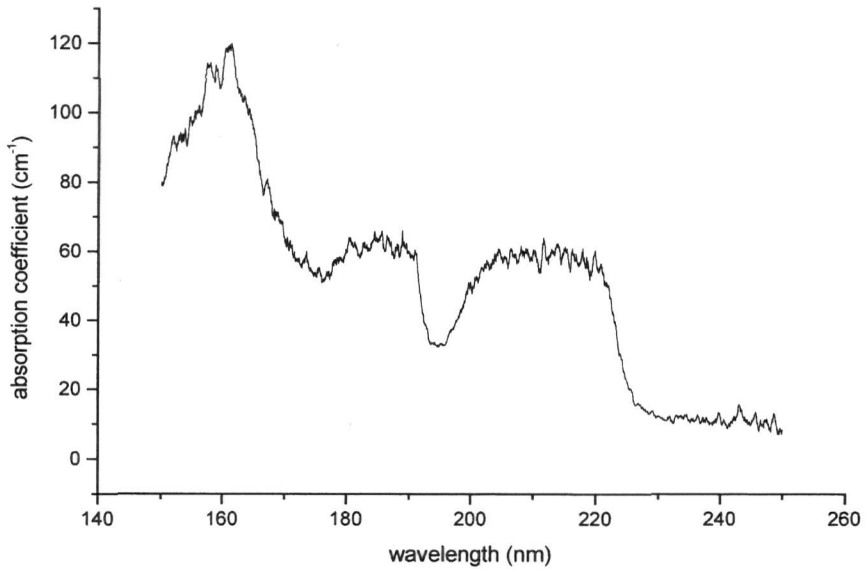
The absorption spectrum of the trivalent Nd^{3+} ion in the VUV has been studied previously in different dielectric crystal hosts [4,7,10,61,81,82,109,115,116]. The energy position of the levels of the $4f^25d$ electronic configuration of the free Nd^{3+} ion can be estimated from data available for the isoelectronic Pr^{2+} . According to

Table 4 Number of Electric Dipole-Allowed Interconfigurational Transitions of Trivalent RE Ions Between the Ground State of the $4f^n$ Electronic Configuration and the Excited Terms of the $4f^{n-1}5d$ Electronic Configuration

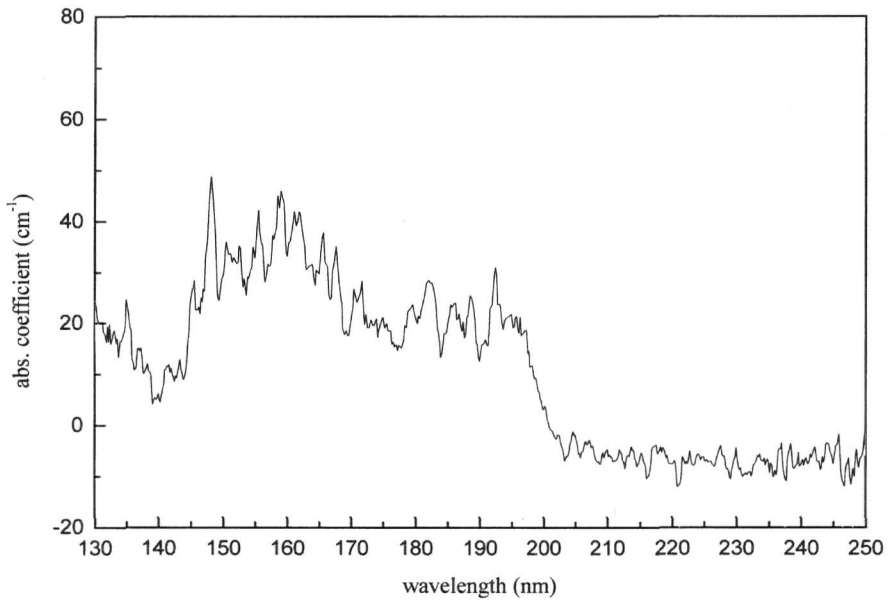
Ion	4f ⁿ configuration		4f ⁿ⁻¹ 5d configuration					
	n	Number of levels	Ground state	Number of levels	Lowest level	Dipole allowed transitions $\Delta S = 0, \Delta L = 0 \pm 1, \Delta J = \Delta J$		
						Excited terms	Terms in tetragonal crystal field	Transitions
La ³⁺	0	1	¹ S ₀	0	—	—	—	0
Ce ³⁺	1	2	² F _{5/2}	2	² D _{3/2}	² D _{3/2}	Γ ₆ + Γ ₇	2
Pr ³⁺	2	13	³ H ₄	20	¹ G ₄	³ G ₃ ³ H ₄	Γ ₂ + Γ ₃ + Γ ₄ + 2Γ ₅ 2 Γ ₁ + Γ ₂ + Γ ₃ + Γ ₄ + 2Γ ₅	5
Nd ³⁺	3	41	⁴ I _{9/2}	107	⁴ I _{9/2}	⁴ H _{7/2} (2) ⁴ I _{9/2}	2Γ ₆ + 2Γ ₇ 3 Γ ₆ + 2Γ ₇	9
Pm ³⁺	4	107	⁵ I ₄	386	⁵ L ₆	⁴ K _{11/2} ⁵ H ₃ (3) ⁵ I ₄ (2)	3Γ ₆ + 3Γ ₇ Γ ₂ + Γ ₃ + Γ ₄ + 2Γ ₅ 2Γ ₁ + Γ ₂ + Γ ₃ + Γ ₄ + 2Γ ₅	14
Sm ³⁺	5	198	⁶ H _{5/2}	977	⁶ L _{11/2}	⁵ K ₅ ⁶ G _{3/2} (4) ⁶ H _{5/2} (3) ⁶ I _{7/2} (2)	Γ ₁ + 2Γ ₂ + Γ ₃ + Γ ₄ + 3Γ ₅ Γ ₆ + Γ ₇ Γ ₆ + 2Γ ₇ 2Γ ₆ + 2Γ ₇	20
Eu ³⁺	6	295	⁷ F ₀	1876	⁷ K ₄	⁷ D ₁ (2) ⁷ F ₁ (3) ⁷ G ₁ (2)	Γ ₂ + Γ ₅ Γ ₂ + Γ ₅ Γ ₂ + Γ ₅	7
Gd ³⁺	7	327	⁸ S _{7/2}	2725	⁸ H _{3/2}	⁸ P _{9/2}	3Γ ₆ + 2Γ ₇	3

Tb ³⁺	8	295	⁷ F ₆	3106	⁹ D ₂	⁷ D ₅ (5) ⁷ F ₆ (5) ⁷ G ₇ (5)	Γ ₁ + 2Γ ₂ + Γ ₃ + Γ ₄ + 3Γ ₅ 2Γ ₁ + Γ ₂ + 2Γ ₃ + 2Γ ₄ + 3Γ ₅ Γ ₁ + 2Γ ₂ + 2Γ ₃ + 2Γ ₄ + 4Γ ₅	30
Dy ³⁺	9	198	⁶ H _{15/2}	2725	⁸ G _{15/2}	⁶ G _{13/2} (11) ⁶ H _{15/2} (10) ⁶ I _{17/2} (9)	3Γ ₆ + 4Γ ₇ 4Γ ₆ + 4Γ ₇ 5Γ ₆ + 4Γ ₇	58
Ho ³⁺	10	107	⁵ I ₈	1876	⁷ H ₈	⁵ H ₇ (18) ⁵ I ₈ (14) ⁵ K ₉ (11)	Γ ₁ + 2Γ ₂ + 2Γ ₃ + 2Γ ₄ + 4Γ ₅ 3Γ ₁ + 2Γ ₂ + 2Γ ₃ + 2Γ ₄ + 4Γ ₅ 2Γ ₁ + 2Γ ₂ + 2Γ ₃ + 2Γ ₄ + 4Γ ₅	79
Er ³⁺	11	41	⁴ I _{15/2}	977	⁶ L _{17/2}	⁴ H _{13/2} (18) ⁴ I _{15/2} (14) ⁴ K _{17/2} (11)	3Γ ₆ + 4Γ ₇ 4Γ ₆ + 4Γ ₇ 5Γ ₆ + 3Γ ₇	79
Tm ³⁺	12	13	³ H ₆	386	⁵ L ₆	³ G ₅ (13) ³ H ₆ (11) ³ I ₇ (9)	Γ ₁ + 2Γ ₂ + Γ ₃ + Γ ₄ + 3Γ ₅ 2Γ ₁ + Γ ₂ + 2Γ ₃ + 2Γ ₄ + 3Γ ₅ Γ ₁ + 2Γ ₂ + 2Γ ₃ + 2Γ ₄ + 4Γ ₅	62
Yb ³⁺	13	2	² F _{7/2}	107	⁴ H _{9/2}	² D _{5/2} (5) ² F _{7/2} (5) ² G _{9/2} (5)	Γ ₆ + 2Γ ₇ 2Γ ₆ + 2Γ ₇ 3Γ ₆ + 2Γ ₇	25
Lu ³⁺	14	1	¹ S ₀	20	³ P ₂	¹ P ₁	Γ ₂ + Γ ₅	1

The number of dipole-allowed transitions is calculated taking into consideration partial restoration of the spherical symmetry for the 5d electronic configuration. The theoretical predictions are in excellent agreement with experimental results.



(a)



(b)

Figure 5 a. VUV absorption spectrum of the $\text{KY}_3\text{F}_{10}:\text{Pr}^{3+}$ crystal. b. VUV absorption spectrum of $\text{LaF}_3:\text{Pr}^{3+}$ crystal.

Sugar [117], 107 possible energy levels exist in the free Pr^{2+} ion of the $4f^25d$ electronic configuration. Among them, only nine levels, $4f^2(^3\text{F})5d$ [$^4\text{H}_{7/2}$, $^4\text{H}_{9/2}$, $^4\text{H}_{11/2}$] and $4f^2(^3\text{H})5d$ [$^4\text{H}_{7/2}$, $^4\text{H}_{9/2}$, $^4\text{H}_{11/2}$, $^4\text{I}_{9/2}$, $^4\text{I}_{11/2}$, $^4\text{K}_{11/2}$], are excited from the ground level $^4\text{I}_{9/2}$ of the $4f^3$ electronic configuration. In order to assign the dipole-allowed transitions between the Stark components of the $4f^25d$ electronic configuration and the levels of the $4f^3$ electronic configuration, the exact solution of the secular equation of the $4f^25d$ electronic configuration in the presence of the crystal field should be known. However up to now, there have been no theoretical calculations regarding the energy position of the levels of the $4f^25d$ electronic configuration.

To find the total number of interconfigurational dipole-allowed transitions of the Nd^{3+} ions, spectral terms that arise from the $5d$ and the $4f$ orbital are formed, followed by calculation of the effect of the crystal field on the system's Hamiltonian. The crystal field divides these nine levels into a total number of 40 Stark components for a C_{4v} or S_4 site symmetry. However if the selection rules for dipole transitions $\Delta S = 0$, $\Delta l = +1, -1$, $\Delta L = 0, +1, -1$, $\Delta J = 0, +1, -1$ ($J = 0 \rightarrow J = 0$ forbidden) and $\Delta J = \Delta L$ are applied, only 11 transitions remain after excitation from the ground level $^4\text{I}_{9/2}$ and the $4f^2(^3\text{F})5d$ [$^4\text{K}_{11/2}$] level is the lowest. The $4f^2(^3\text{H})5d$ [$^4\text{H}_{7/2}$] level is the highest. In the case of Nd^{3+} ion in LiYF_4 crystal hosts (C_{4h} space symmetry group, S_4 point symmetry group of the Nd^{3+} ions), 11 Stark components are populated through dipole-allowed transitions from the ground level $^4\text{I}_{9/2}$ of the $4f^3$ electronic configuration, which is in excellent agreement with the experiments [82].

Therefore, the charge compensation and localized character of the d orbitals partially restore the spherical symmetry of angular momentum. In this case, the main effect of a strong crystal field is to lower the energy levels of the $4f^{n-1}5d$ electronic configuration relative to the free ion case. The amount of shifting is directly correlated to the magnitude of the crystal field. The absorption spectrum was slightly broadened at room temperature compared to lower temperature (77 K). The structure of the spectrum verifies the mixed character of the $4f^25d$ electronic configuration and partial restoration of the spherical symmetry. The absorption peak around $66,578 \text{ cm}^{-1}$ probably has a weak additional contribution from the highly excited levels of the Nd^{3+} ion of the $4f^3(^2\text{F})$ electronic configuration [29]. In this experiment the band gap of the LiYF_4 crystal host was estimated to be $86,900 \text{ cm}^{-1}$ wide (for a 0.5 mm thick crystal). However, the value of the band gap is estimated to be wider for a thinner sample. The absorption band from 115 to 118 nm has been observed for various host lattices. It was attributed to transitions between the valence and the conduction band of the host lattice. In condensed matter at room and low temperatures, dipole transitions between the ground level of the Nd^{3+} ion and the levels of the $4f^25d$ electronic configuration usually have a broad band structure, due to the wide spatial distribution of the electronic cloud. A similar response is expected for crystal hosts of different

symmetry. For example, in the case of the rhombic PFYK:Nd crystal (space group Pnam) [118], absorption spectrum showed that the $4f^25d$ configuration levels split into nine main Stark components with maximum absorption at 56,212; 58,423; 59,180; 62,606; 65,789; 66,906; 70,061; 74,174; and 79,878 cm^{-1} , respectively [82]. The absorption spectrum of the $\text{LiCaAlF}_6:\text{Nd}^{3+}$ crystal in the spectral range from 120 to 200 nm is likewise indicated in Figure 6. The peaks were assigned to strong dipole-allowed transitions between the $^4I_{9/2}$ ground level of the $4f^3$ electronic configuration and the Stark components of the levels of the $4f^25d$ electronic configuration.

When the crystal field of trigonal symmetry is applied, on the $^4K_{11/2}$ level of the Nd^{3+} free ion, it splits it into three Stark components: $2(\Gamma^{(4)} + \Gamma^{(5)} + \Gamma^{(6)})$, $\Gamma^{(4)}$, $\Gamma^{(4)}$. The $^4I_{9/2}$ level likewise splits into two Stark components by the trigonal crystal field: $2(\Gamma^{(4)} + \Gamma^{(5)} + \Gamma^{(6)})$, $\Gamma^{(4)}$. The $^4H_{7/2}$ splits into three Stark components: the $\Gamma^{(4)}$, $\Gamma^{(4)}$, $(\Gamma^{(4)} + \Gamma^{(5)} + \Gamma^{(6)})$. Some of these components are degenerate and the degeneracy is removed within the $4f^25d$ electronic configuration. In the case of trigonal symmetry, the dipole-allowed transitions between the ground state $^4I_{9/2}$ of the $4f^3$ electronic configuration and the Stark components

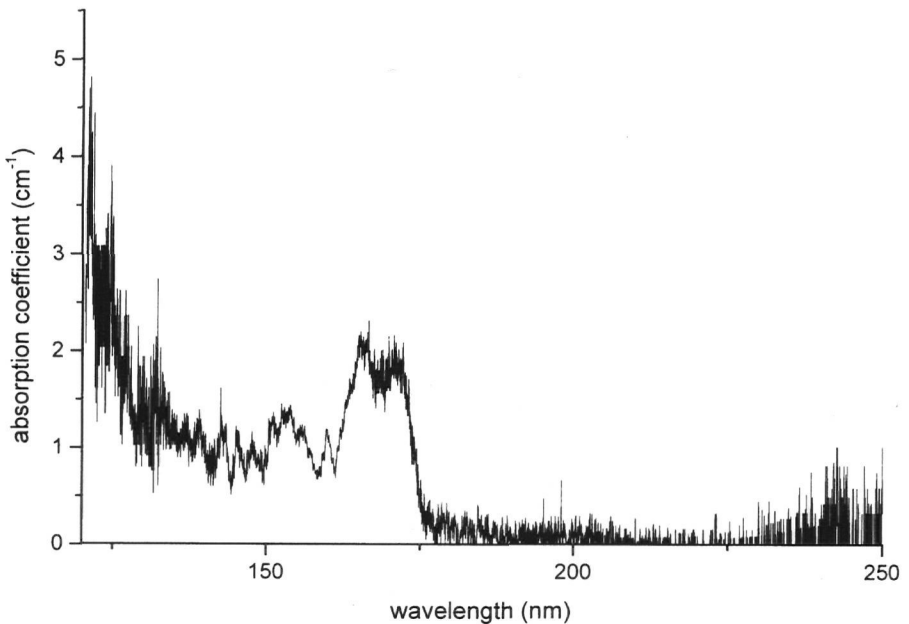


Figure 6 Absorption spectrum of $\text{LiCaAlF}_6:\text{Nd}^{3+}$ crystal in the spectral region from 120 to 250 nm.

of the $4f^25d$ electronic configuration are 20, in agreement with experimental observations. The peak at 115 nm corresponds to excitonic transitions between the valence and conduction band of the host lattice, suggesting a large value of the index of refraction, which is in agreement with previous measurements of fluoride crystals' than films in the VUV.

D. Promethium (Pm^{3+} , $4f^4$)

Promethium is an artificial element that is highly radioactive. The $4f^4$ electronic configuration of Pm^{3+} ions has been investigated in $LaCl_3$ crystals [119,120]. There are 107 and 386 levels of the $4f^4$ and the $4f^35d$ electronic configurations respectively. In the free ion case, 5L_6 is the lowest level of the $4f^35d$ electronic configuration. Six terms—the 3H (3), 5I , and 5K —are excited through dipole-allowed transitions from the ground state 5I_4 of the $4f^4$ electronic configuration. Fourteen dipole-allowed transitions are expected in the crystal field with tetragonal symmetry. Free-ion calculations put the edge of the $4f^35d$ electronic configuration at $73,300\text{ cm}^{-1}$ and the $4f^34s$ electronic configuration at $111,000\text{ cm}^{-1}$ [2].

E. Samarium (Sm^{3+} , $4f^5$)

The energy position of the levels of $4f^4 5d$ electronic configuration of free Sm^{3+} ion can be estimated based on the data available for isoelectronic Nd^+ [120,121]. The free Sm^{3+} ion has 977 levels of $4f^45d$ electronic configuration. Among them, only nine terms [four 6G , three 6H , and two 6I] are excited from the ground level $^6H_{5/2}$ of the $4f^5$ electronic configuration, giving 20 dipole-allowed transitions excited from the ground state. The lowest level of the $4f^45d$ electronic configuration is the $^6L_{11/2}$ one at $73,700\text{ cm}^{-1}$ above the ground state. The $4f^5$ electronic configuration of the free ion consists of 198 levels [81]. It has been analyzed in crystals [122,123]. Early measurements of crystal field splitting of single and mixed electronic configurations of Sm ions in various dielectric crystal hosts were attributed to the divalent Sm^{2+} ions [124–126]. The edge of the levels of $4f^45d$ electronic configuration in LaF_3 was at $58,000\text{ cm}^{-1}$ and extends well beyond the cut-off of the crystal host. The VUV absorption spectra of Sm ions in various dielectric crystal hosts, CaF_2 [121,127] and $LiYF_4$ [128], were interpreted as $4f^5 \rightarrow 4f^45d$ interconfigurational transitions of the trivalent Sm^{3+} ions. Absorption spectra of $CaF_2:Sm^{3+}$ are unique in that some spectral lines arising from thermally excited Stark levels of the $4f^5$ electronic configuration were observed at low temperatures [81]. The average spacing between zero phonon and vibronic lines is $\sim 486\text{ cm}^{-1}$. This frequency has been attributed to a local mode between the Sm^{3+} ion and its nearest-neighbor fluorine ions [129].

As already mentioned, the effect of the crystal field on the $4f^{n-1}5d$ electronic configuration energy would be to lower its edge; various empirical methods

have been established [77], based on the following principle: The energy difference Δ between two configurations differing by a single electron in the 4f configuration (e.g., $4f^n$ and $4f^{n-1}5d$) is constant for all the lanthanides. Martin [130] estimated the Δ energy difference for neutral monovalent and divalent ions from a few measured values. Sugar and Reader [131] applied this principle to estimate trivalent ion differences using Martin's results. In the free ion case, the energy difference between the $4f^45d$ and the $4f^5$ levels was estimated to be $76,000 \pm 2000 \text{ cm}^{-1}$ [77,130–131]. In the presence of the CaF_2 crystal field, a depression of the upper configuration by about 18000 cm^{-1} towards the ground state is taking place [92]. Hence the edge of the levels of the $4f^45d$ electronic configuration in the presence of the CaF_2 crystal field is expected to be at $58,000 \pm 2000 \text{ cm}^{-1}$, in agreement with the experiments [121].

F. Europium (Eu^{3+} , $4f^6$)

The free Eu^{3+} ion has 1878 levels [81] of $4f^55d$ electronic configuration. Among them, seven terms [two ${}^7\text{G}$, three ${}^7\text{F}$, and two ${}^7\text{D}$] are excited from the ground level ${}^7\text{F}_0$ of the $4f^6$ electronic configuration, giving seven dipole allowed transitions excited from the ground state. The lowest level of the $4f^55d$ electronic configuration is the ${}^7\text{K}_4$, at $81,800 \text{ cm}^{-1}$ above the ground state ${}^7\text{F}_0$ of the $4f^6$ electronic configuration. The $4f^6$ electronic configuration of the free ion consists of 295 levels [81]. Comparison of the absorption spectrum of CaF_2 : Eu^{3+} ion with an energy level system of the free isoelectronic Sm^{2+} has been given by Schlesinger and Szczurek [121]. The so-called system difference $4f^55d-4f^6$ in the free Eu^{3+} ions was estimated to be $85,500 \pm 1000 \text{ cm}^{-1}$. In the presence of the CaF_2 crystal field, the first level of the $4f^55d$ electronic configuration is expected to be at $67,500 \pm 1000 \text{ cm}^{-1}$, which is in agreement with experimental observations [121]. The vibrational structure has been analyzed from the absorption spectrum and the separation from zero-phonon lines. Their vibronics were found to be $\sim 452 \text{ cm}^{-1}$ and 486 cm^{-1} [121]. The two values were attributed to the formation of centers of different site symmetry and clustering at higher concentration of the RE ions. Strong absorption of Eu^{3+} ions in LaF_3 crystals between 200 and 300 nm has been attributed to interconfigurational transitions from divalent ions [2]. The $5d$ electronic configuration of the Eu^{2+} ion is calculated to begin at $33,900 \text{ cm}^{-1}$ and the $6s$ electronic configuration at $44,300 \text{ cm}^{-1}$ [131].

G. Gadolinium (Gd^{3+} , $4f^7$)

Crosswhite and Kielkopf have studied the free ion spectrum and identified several lines from the $4f^65d$ electronic configuration occurring between $104,000$ and $122,000 \text{ cm}^{-1}$ [132,133]. Despite the fact that Gd^{3+} ions in the $4f^65d$ electronic

configuration have 2725 levels [81], only three among them are important if electric dipole-allowed transitions from the ground state are taken into consideration, the ${}^8P_{5/2}$, ${}^8P_{7/2}$, and ${}^8P_{9/2}$. In free Gd^{3+} ions these levels are expected to be separated from the lowest energy level of the $4f^65d$ electronic configuration, ${}^8H_{3/2}$, by about 8000, 9600, and 11,200 cm^{-1} , respectively [132]. These three levels are spread over the energy range of 3200 cm^{-1} . Separation between the extreme nonphonon lines in the absorption spectrum is about the same, namely 3600 cm^{-1} [134]. The lowest energy level of the $4f^65d$ electronic configuration ${}^8H_{3/2}$, in CaF_2 is situated at 77,760 cm^{-1} , in agreement with Loh's estimation at 78,000 cm^{-1} [92]. In this work, the absorption lines at 77,890 and 79,710 cm^{-1} were assigned to spin-forbidden transitions. The spectrum of Gd^{3+} ions in CaF_2 is exceptional in that it does not seem to exhibit the type of vibronic feature at about 490 cm^{-1} from the parent zero phonon line that appears in the $4f \rightarrow 5d$ absorption spectra of all 10 other triply ionized rare earth ions in CaF_2 .

H. Terbium (Tb^{3+} , $4f^8$)

The absorption spectrum of the trivalent Tb^{3+} ion has been studied previously in different crystal lattices [2,5,83,135]. The electric crystal field splits all the levels of single and mixed configuration. The number and the spacing of the components depend on the symmetry and intensity of the crystal field. Such splitting has been observed previously for the Tb^{3+} ion in other dielectric crystal host materials as well. For example, regarding the $LiYF_4:Tb^{3+}$ crystal (site symmetry C_{4h} or S_4), it was found that the electric crystal field splits the $4f^75d$ electronic configuration into five main Stark components with maximum absorption at 46,700, 51,500, 55,000, 60,600, and 80,900 cm^{-1} , respectively [135]. For the $LaF_3:Tb^{3+}$ crystal (C_2 or D_{3h} site symmetry), the electric crystal field likewise splits the levels of the $4f^75d$ electronic configuration into seven main Stark components with maximum absorption at 54,000, 55,500, 57,800, 58,800, 61,300, 65,800, and 73,000 cm^{-1} respectively [2]. In the case of the free Tb^{3+} ion, Dieke and Crosswhite indicated that the $4f^75d$ electronic configuration splits into two groups of levels, and the energy gap between them extends from 55,700 to 65,000 cm^{-1} [29]. For the LaF_3 crystal, the edge of the levels of the $4f^75d$ configuration is at 50,000 cm^{-1} [19]; for the CaF_2 at 46,500 cm^{-1} [19]; and around 44,900 cm^{-1} for the $LiYF_4$ crystal [18]. The edge of the levels of the $4f^75d$ electronic configuration in the case of the free Tb^{3+} ion is at 54,900 cm^{-1} [23].

According to Szczurek and Schlesinger [81], the $4f^7$ electronic configuration of the Tb^{3+} ion is half-filled, and the lower energy level of the $4f^75d$ electronic configuration is the ${}^8S_{7/2}$ one, which has zero total angular momentum. Therefore, in a pure L-S coupling the 5d electron does not interact with the $4f^7$ shell. The interaction is taking place only through the crystal field. In this aspect the Tb^{3+} ion is similar to the Ce^{3+} ion, although the last one in the 5d electronic

configuration has an empty 4f shell. As a result, the low-energy part of the absorption spectrum of the Tb^{3+} ions in the $4f^75d$ electronic configuration should be quite similar to that of Ce^{3+} ions. The absorption spectra of $\text{LiLuF}_4: \text{Tb}^{3+}$ in the 140–220 nm spectral range consists of a band displaying similar structure to the spectrum of Ce^{3+} ions in crystal field in the 180–320 nm spectral range. The separation between the extreme lines in the spectra is about $20,600 \text{ cm}^{-1}$ for terbium and about $21,600 \text{ cm}^{-1}$ for cerium. This experimental evidence supports the argument that in both cases the lowest energy-level system in the $4f^{n-1}5d$ electronic configuration is formed through the interaction between the 5d electron and the crystal field. Following this argument and taking into consideration that spherical symmetry is partially restored, the $4f^7(^8\text{S})5d$ electronic configuration consists of two terms, the ^9D and the ^7D one, and only the $^7\text{D}_5$ is populated through the electric dipole transitions from the $4f^8(^7\text{F}_6)$ ground level of the $4f^8$ electronic configuration. The crystal field of tetragonal symmetry should split the $^7\text{D}_5$ level into eight Stark components ($^7\text{D}_5 = \Gamma_1 + 2\Gamma_2 + \Gamma_3 + \Gamma_4 + 3\Gamma_5$).

In order to find the relative energy position of the Stark components, it is necessary to construct the basic functions for the Γ_{1-5} irreducible representations, and then to calculate the matrix elements of the electrostatic potential on the Tb^{3+} ion, for each one of the eight Stark components. In this approximation, the total angular momentum, J , is the good quantum number (J – J coupling). However in order to avoid the lengthy calculations, a different approach can be applied that considers the orbital angular momentum of the d electron ($L = 2$) to be the good quantum number. In this first-order approximation, the Γ_4 irreducible representation has the lowest energy in a tetragonal site symmetry. The next irreducible representation with higher energy to the Γ_4 , is the Γ_5 one, followed by the Γ_3 and the Γ_1 . The Γ_2 and the Γ_5 Stark components are double and triple degenerate. The degeneracy can be raised when the L–S coupling strength is strong enough within the levels of the $4f^75d$ electronic configuration. The splitting of the levels of the $4f^75d$ electronic configuration due to the L–S coupling is only few hundred wavenumbers, and this value is considerably smaller than the crystal field splitting. In the case of the $\text{LiYF}_4:\text{Tb}^{3+}$ ions, the eight Stark components of the $^7\text{D}_5$ level were assigned to the levels of the $4f^75d$ electronic configuration at 47,000, 52,000, 54,400, 55,500, 55,900, 62,200, 64,300, and $67,500 \text{ cm}^{-1}$ respectively [135]. We therefore assign the triple degenerate Γ_5 Stark component to the energy levels at 54,400, 55,500, and $55,900 \text{ cm}^{-1}$, and the double degenerate Γ_2 Stark component to the energy levels at 62,200 and $64,300 \text{ cm}^{-1}$, respectively. The remaining three Stark components Γ_1 , Γ_3 , and Γ_4 were assigned to the energy levels at 67,400, 52,000, and $47,000 \text{ cm}^{-1}$, respectively. The next to the lowest ^8S level of the $4f^75d$ electronic configuration is the $4f^7(^6\text{P})5d$ one. The exact value of the separation between the ^6S and the ^6P levels of the $4f^7$ electronic configuration is not known exactly, but it might be assumed to be of the same order of magnitude as in the case of the Gd^{3+} ions, which is $32,000 \text{ cm}^{-1}$ [24].

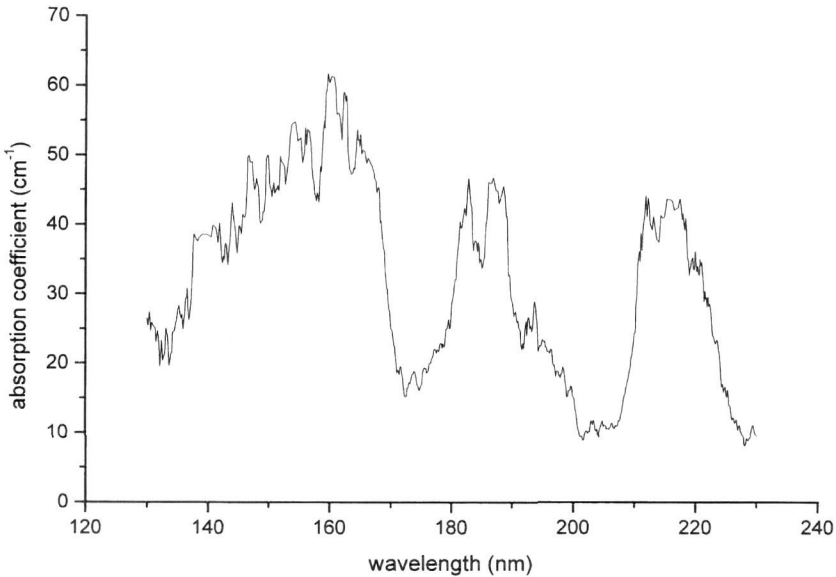


Figure 7 VUV absorption spectrum of $\text{K}_2\text{YF}_5:\text{Tb}^{3+}$.

The $4f^7(6P)5d$ electronic configuration has four terms that are excited from the 7F_6 ground level of the $4f^8$ electronic configuration: the 7F_6 , 7F_5 , 7G_7 and the 7G_6 ones. The crystal field splits all these levels to a total number of 26 Stark components for a C_{4v} or an S_4 site symmetry. However, if the selection rules for dipole transitions $\Delta S = 0$, $\Delta L = \pm 1$, $\Delta L = 0, \pm 1$, $\Delta J = 0, \pm 1$, ($J = 0 \rightarrow J = 0$ forbidden), and $\Delta J = \Delta L$ applied, only 14 transitions remain after the excitation from the ground level 7F_6 , which occupies the spectral region from 120 to 240 nm.

A similar structure has been observed previously for the $\text{LiYF}_4:\text{Tb}^{3+}$ crystal in this spectral range [135]. The band gap of the LiLuF_4 crystal was estimated to be $77,600 \text{ cm}^{-1}$ wide. It is possible the levels of the $4f^75d$ electronic configuration overlap with the levels of the $4f^76s$ electronic configuration below 120 nm [2]. The VUV spectrum of the Tb^{3+} ions in K_2YF_5 crystal hosts is indicated in Figure 7. The spectrum is similar to that of the $\text{LiYF}_4:\text{Tb}^{3+}$ crystal [135].

I. Dysprosium (Dy^{3+} , $4f^9$)

The $4f^9$ electronic configuration of trivalent dysprosium in LaF_3 indicated a complex structure. The edge of the levels of the $4f^85d$ electronic configuration of free trivalent dysprosium ions is calculated to be at $66,300 \text{ cm}^{-1}$ and at $99,100 \text{ cm}^{-1}$ for the $6s$ electronic configuration. The absorption spectrum of Dy^{3+} ions

in LaF_3 indicates a complex structure [136] and accurate assignment of states has not been made above $24,000 \text{ cm}^{-1}$. The VUV absorption spectrum of the Dy^{3+} ions in CaF_2 begins at 175 nm and consists of many sharp zero-phonon lines and elaborately structured phonon side bands. There are two peaks in the VUV absorption spectrum of Dy^{3+} ions in CaF_2 situated at 490 and 100 cm^{-1} from their parent zero-phonon lines [137]. The peak at 490 cm^{-1} is attributed to a localized vibrational mode of the eight nearest fluorine neighbors of the Dy^{3+} ions. The vibration mode at 490 cm^{-1} is present in CaF_2 crystals doped with different RE ions such as Ce^{3+} , Tb^{3+} , and Ho^{3+} ions.

J. Holmium (Ho^{3+} , $4f^{10}$)

The absorption spectrum of the trivalent Ho^{3+} ion was studied previously in a number of crystal lattices [2,7,81,138,139]. The electric crystal field splits all the levels of the single and the mixed configurations. Three Stark components of the levels of the $4f^95d$ electronic configuration were observed previously in the case of the BaY_2F_8 crystal host, with maximum absorption at $63,900 \text{ cm}^{-1}$ (156.4 nm), $67,800 \text{ cm}^{-1}$ (147.4 nm), and $71,800 \text{ cm}^{-1}$ (139.2 nm). The edge of the levels of the $4f^95d$ electronic configuration was found to be at $63,100 \text{ cm}^{-1}$ (158.4 nm) [139]. For the LaF_3 and the CaF_2 crystal hosts, the edges of the levels of the $4f^95d$ electronic configuration for the spin-allowed transitions were found to be at $63,300 \text{ cm}^{-1}$ (158.7 nm) and $64,100 \text{ cm}^{-1}$ (156.0 nm), respectively [2,138]. For the free ion case, the edge of the levels of the $4f^95d$ electronic configuration was found to be at $58,900 \text{ cm}^{-1}$ (169.5 nm) [29]. In the case of the single LiYF_4 crystal and for 0.1 at. % concentration of the Ho^{3+} ions, the edge of the levels of the $4f^95d$ electronic configuration for the spin-allowed transitions was found to be at $63,300 \text{ cm}^{-1}$ (158 nm) [174]. In the spectral range from 120 to 158 nm, five main Stark components of the $4f^95d$ electronic configuration with maximum absorption at $64,800 \text{ cm}^{-1}$ (153.4 nm), $69,300 \text{ cm}^{-1}$ (143.5 nm), $73,200 \text{ cm}^{-1}$ (136.6 nm), $78,900 \text{ cm}^{-1}$ (126.7 nm), and $84,100 \text{ cm}^{-1}$ (118.8 nm) were observed.

In the spectral range from 158 to 170 nm, four main Stark components of the $4f^95d$ electronic configuration with maximum absorption at $59,700 \text{ cm}^{-1}$ (167.5 nm), $60,200 \text{ cm}^{-1}$ (166 nm), $61,200 \text{ cm}^{-1}$ (163 nm), and $61,900 \text{ cm}^{-1}$ (162 nm) were likewise observed. They were assigned previously to spin-forbidden transitions [128]. This assignment was justified because of the low value of the absorption coefficient, in comparison to the value of the absorption coefficient for wavelengths less than 158 nm, and on the other hand because of the long lifetime (300 ns) of the corresponding transitions. The transitions between $58,800 \text{ cm}^{-1}$ (170 nm) and $54,400 \text{ cm}^{-1}$ (184 nm) were assigned to the $4f^{10} \rightarrow 4f^{10}$ intraconfigurational dipole-forbidden transitions.

The local maximum around 116 nm [175] is attributed to the transition between the valence and the conduction bands of the host lattice. From the ab-

sorption spectrum it is estimated that the band gap of the LiYF_4 crystal host is $86,200 \text{ cm}^{-1}$ (116 nm) wide. This value is in agreement with the value of the band gap of 10.7 eV (115 nm) of the LiYF_4 crystal, estimated previously from reflection spectra [3]. Indeed, the cut-off wavelength of the LiF window, which is placed in front of the hydrogen lamp and the solar blind photomultiplier, is at 110 nm. The transmittance of the LiF window drops successively from its highest value at 120 nm, to zero at 110 nm when it is recorded using a secondary electron multiplier of open geometry without the $\text{LiYF}_4:\text{Ho}^{3+}$ crystal in the optical path. In this spectral region, there is only one local maximum at 112 nm. When the transmittance is recorded with the the $\text{LiYF}_4:\text{Ho}^{3+}$ crystal in the optical path, two new additional local maxima appear in the absorption spectrum from 110 to 120 nm, one at 116 nm and the other at 118.8 nm. A local maximum around 116 nm appears as well in the absorption spectrum of LiYF_4 crystals doped with Nd^{3+} ions [3,82]. Hence the position of the local maximum at 116 nm should be independent of the RE dopands in LiYF_4 crystal hosts and it is assigned to a transition between the valance and the conduction band of the LiYF_4 crystal.

There is not a sharp transition between the valance and the conduction band due to the delocalized nature of the conduction band. From the absorption spectrum, the oscillation strength of the transition between the valance and the conduction band increases as one shift in the wavelength scale from 122 to 116 nm. For wavelengths less than 122 nm, the levels of the $4f^95d$ electronic configuration of the Ho^{3+} ions are mixed with the delocalized levels of the conduction band of the crystal host, and the transmittance of the crystal decreases rapidly in this spectral region. Hence, the absorption spectrum between 110 and 122 nm, indicates only the position of the levels of $4f^95d$ electronic configuration inside the conduction band. In this case the value of the absorption coefficient cannot be calculated, because of the low value of the signal-to-noise ratio of the light source, which approaches unity. The absorption peak at 122 nm corresponds to the transition between the $^5\text{I}_8$ ground level of the $4f^{10}$ electronic configuration and the edge of the conduction band. Therefore the position of the $^5\text{I}_8$ ground level of the Ho^{3+} ion is $4200 \pm 800 \text{ cm}^{-1}$ above the top of the valance band of the LiYF_4 crystal host, provided that the band gap of the LiYF_4 crystal is $86,200 \text{ cm}^{-1}$ wide. The local maximum at 118.5 nm likewise corresponds either to the transition between the ground $^5\text{I}_8$ level and a Stark component of the $4f^95d$ electronic configuration inside the conduction band or to a transition from the ground $^5\text{I}_8$ level to a localized level inside the conduction band.

K. Erbium (Er^{3+} , $4f^{11}$)

The edge of the levels of the $4f^{10}5d$ electronic configuration of the Er^{3+} ions was calculated to be at $75,400 \text{ cm}^{-1}$ [131]. The lowest level of the $4f^{10}5d$ electronic

configuration is the ${}^6L_{17/2}$ and 79 dipole-allowed transitions are excited from the ground state ${}^4I_{15/2}$ of the $4f^{11}$ electronic configuration. The absorption spectrum of the trivalent Er^{3+} ion in the VUV has been studied previously in a number of crystal lattices [1–3,9,81,140–141] and it was found to be rather simple, mainly because very few energy levels of the $4f^{10}5d$ electronic configuration are within the band gap of the host material. Intraconfigurational VUV dipole-forbidden $4f^{11} \rightarrow 4f^{11}$ transitions of Er^{3+} ions were observed in various dielectric crystals as well [142]. The edge of the levels of the $4f^{10}5d$ electronic configuration in KY_3F_{10} host was found to be at $60,850 \text{ cm}^{-1}$. Five absorption bands of the $4f^{10}5d$ electronic configuration have been observed in BaY_2F_8 hosts with the maximum of the absorption at $63,700$, $67,900$, $70,500$, $73,400$, and $74,600 \text{ cm}^{-1}$. The edge of the levels of the $4f^{10}5d$ electronic configuration in this crystal host was found to be at $61,900 \text{ cm}^{-1}$, $58,000 \text{ cm}^{-1}$ in LaF_3 [2], and at $63,000 \text{ cm}^{-1}$ in LiLuF_4 [9]. Five main Stark components of the $4f^{10}5d$ electronic configuration have been observed as well in LiLuF_4 hosts with the maximum of the absorption at $60,980$, $69,198$, $71,422$, $74,343$, and $76,916 \text{ cm}^{-1}$. The presence of an additional weak absorption band with maximum of absorption at 163 nm in LiLuF_4 host has been observed as well by Devyatkova et al. [141] in KY_3F_{10} matrices at 164.4 nm .

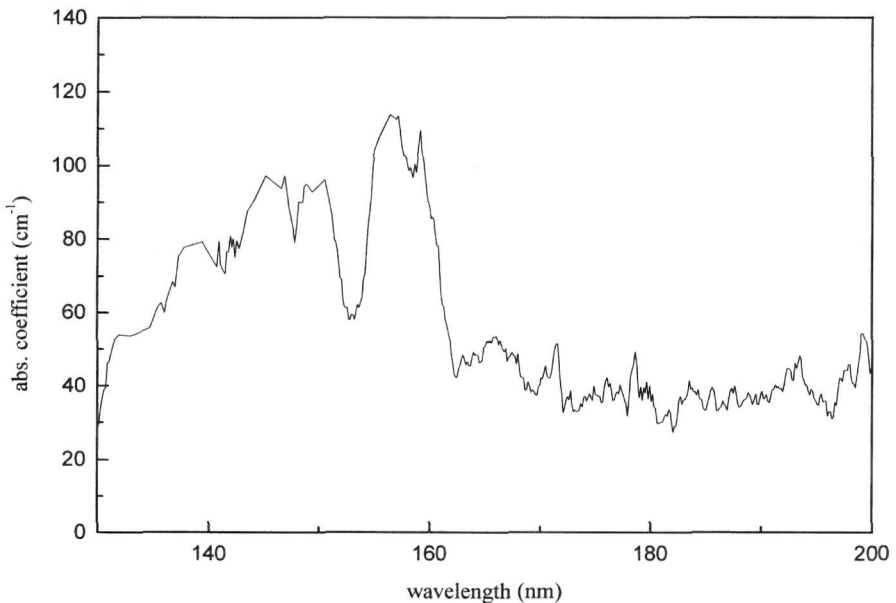


Figure 8 VUV absorption spectrum of $\text{K}_2\text{YF}_5:\text{Er}^{3+}$ crystals.

The VUV absorption spectrum of the Er^{3+} ions in K_2YF_5 crystal hosts is indicated in Figure 8.

L. Thulium (Tm^{3+} , $4f^{12}$)

The edge of the levels of the $4f^{11}5d$ electronic configuration of the free Tm^{3+} ions was estimated to be at $74,300\text{ cm}^{-1}$, and that of the $4f^{11}6s$ electronic configuration at $101,300\text{ cm}^{-1}$ [29]. The relative simplicity of the spectrum in various dielectric hosts arises because only some of the levels of the $4f^{11}5d$ electronic configuration lay below the edge of the conduction band. The absorption spectrum of Tm^{3+} ions in LiLuF_4 [135] indicates the presence of four bands with maximum of absorption at $63,300$, $69,000$, $73,000$ and $76,500\text{ cm}^{-1}$, respectively and for the K_2YF_5 host the VUV absorption spectrum of the Tm^{3+} ions is indicated in Figure 9. VUV absorption spectra of Tm^{3+} ions in different fluoride dielectric hosts have been analyzed by Szczurek and Schlesinger [143–145]. The main result of these investigations was that different possible transitions and

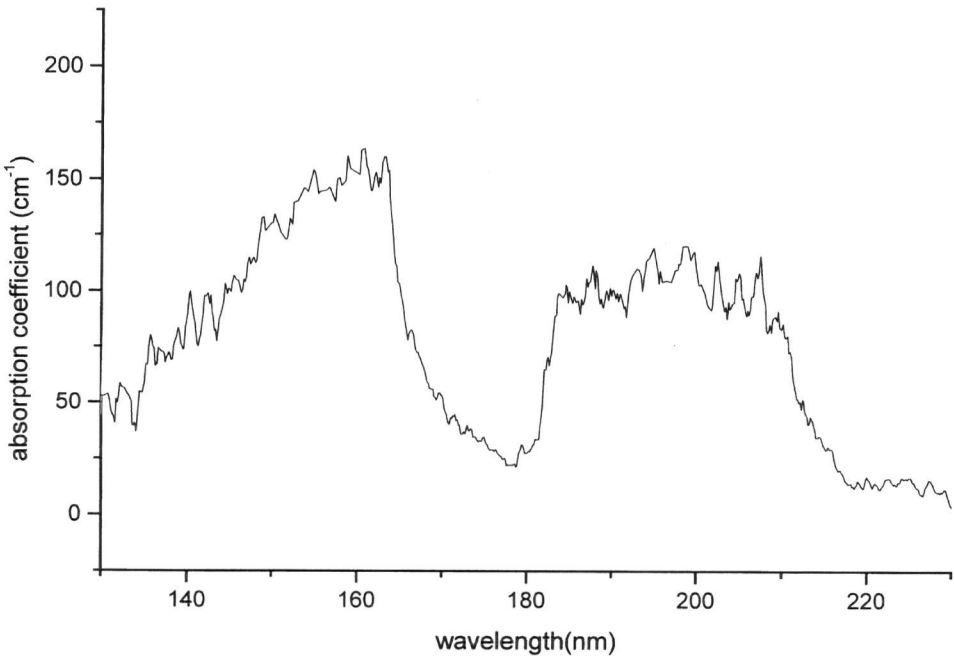


Figure 9 VUV absorption spectrum of the $\text{K}_2\text{YF}_5:\text{Tm}^{3+}$ crystal.

relaxation paths are dependent upon lattice temperature. The temperature-dependent lifetimes can be expected to occur as a result of phonon-assisted radiative transitions.

M. Ytterbium (Yb^{3+} , $4f^{13}$)

The free Yb^{3+} in the $4f^{12}5d$ electronic configuration has 107 energy levels. Among these, some 20 levels have been measured from gaseous spectra [146] including the lowest $^4\text{H}_{9/2}$ level. This enables one to make some limited comparison of the observed spectra of Yb^{3+} in different crystal hosts with the free Yb^{3+} energy levels [147–149]. The crystal field of the C_{4v} symmetry splits the lowest $^4\text{H}_{9/2}$ level into five Stark levels. The separation between the extreme of these five lines is about 2100 cm^{-1} . This value is about one order of magnitude smaller than the corresponding $4f^{n-1}5d$ level splitting observed, for instance, in cerium, praseodymium, or terbium. This suggests that the interaction between the $5d$ electron and the crystal field is weak.

IV. LASER-INDUCED FLUORESCENCE OF RE IONS IN WIDE BAND GAP FLUORIDE CRYSTALS AT 157 nm

When the RE ion is excited from its ground level of the $4f^n$ electronic configuration to a given level of the $4f^{n-1}5d$ electronic configuration, it populates the levels of the $4f^n$ electronic configuration from the edge and the Stark components of the levels of the $4f^{n-1}5d$ electronic configuration. This is a rather common response to photoexcitation of the trivalent RE ions in fluoride dielectric crystals, and it has been observed previously for other dielectric crystals doped with RE ions [9,82,150]. In this case competition starts between radiative and nonradiative transitions. The nonradiative transitions are faster and usually the ion will decay to the lowest of the $4f^{n-1}5d$ levels. The transitions arising from the edge and the levels of the $4f^{n-1}5d$ electronic configuration and the laser induced fluorescence (LIF) spectrum could be interpreted on the basis of four different processes:

1. The formation of optically active RE centers of different site symmetries, which always are present at high concentration of the RE ions [151].
2. Direct $4f^{n-1}5d \rightarrow 4f^n$ emission from the levels of the $4f^{n-1}5d$ electronic configuration due to large energy separation of the $4f^{n-1}5d$ levels and/or weak electron [$4f^{n-1}5d$]-phonon interaction.
3. Emission from the levels of the $4f^{n-1}5d$ electronic configuration due to the repopulation of these levels via phonon trapping and reabsorp-

tion of the lattice vibrations within the levels of the $4f^{n-1}5d$ electronic configuration.

4. Spin-forbidden transitions.

Direct emission from the Stark components of the levels of the $4f^{n-1}5d$ electronic configuration should be taking place only when: (1) two successive electronic levels are well separated by the combined energy of a few phonons (e.g., the phonon energy of LiYF_4 crystal is between 140 and 500 cm^{-1} [152]); (2) the energy separation is larger than kT ; and (3) the strength of the electron [$4f^{n-1}5d$]-phonon interaction is weak.

For example, in the case of the Ho^{3+} ions, there are 1878 electronic levels of the $4f^95d$ electronic configuration in the energy range from $80,000$ to $60,000\text{ cm}^{-1}$. Therefore, two successive electronic levels are separated by 11 cm^{-1} (assuming an even distribution of the electronic energy levels over the spectral range). Because the phonon energies of the LiYF_4 crystal are higher than 150 cm^{-1} [153], there is a small probability of direct transitions between the Stark components of the levels of the $4f^95d$ electronic configuration and the levels of the $4f^{10}$ electronic configuration. The interconfigurational $4f^95d \rightarrow 4f^{10}$ transitions in this case are taking place from the edge of the levels of the $4f^95d$ electronic configuration.

For those of the RE ions with weak electron [$4f^{n-1}5d$]-phonon interaction, the coupling strength of the interaction is described within the validity of the Born-Oppenheimer approximation. In this case, radiationless transitions within the levels of the $4f^{n-1}5d$ electronic configuration with a different set of good quantum numbers are forbidden. Therefore, the probability for interconfigurational radiative transitions, which originate directly from the levels of the $4f^{n-1}5d$ electronic configuration, is expected to be high for those of the RE ions where the electron [$4f^{n-1}5d$]-phonon interaction is weak. This situation is confirmed by experimental observations in the case of the Tb^{3+} [83], Gd^{3+} [22], and Er^{3+} [9,128] ions. On the contrary, in the case of strong electron-phonon interaction, as for the Pr^{3+} [8], Nd^{3+} [82], and Ho^{3+} [7] ions, the rate of the internal relaxation within the levels of the $4f^{n-1}5d$ electronic configuration is expected to be high. In this case the dipole-allowed transitions are expected to originate mainly from the edge of the levels of the $4f^{n-1}5d$ electronic configuration.

In addition, for those of the RE ions with strong electron-phonon interaction [5,153–155], dipole-allowed transitions directly from inside the levels (Stark components) of the $4f^{n-1}5d$ electronic configuration could be explained on the basis of the repopulation of these levels through phonon reabsorption and trapping within the levels of the $4f^{n-1}5d$ electronic configuration [82]. The repopulating process will cease when the trapped phonons escape from the active volume by frequency shifting through the dipole-allowed $4f^{n-1}5d \rightarrow 4f^n$ interconfigurational transitions. Finally, the spin allowed and the spin-forbidden [150] intercon-

figurational transitions can be explained on the basis of selection rules and rates of relaxation within the levels of the $4f^{n-1}5d$ electronic configuration.

A. Cerium

There is much interest in Ce^{3+} -doped ionic crystals for applications in UV scintillators [150–160] and lasers [13–15,26]. Cerium trivalent ions in various dielectric crystal hosts are characterized by excellent photochemical stability, high conversion efficiency, and low excited-state absorption coefficient. They also exhibit broadband tunable positive gain in UV, such as in $LiCaAlF_6$ crystal hosts [161,162]. Polarized luminescence and absorption spectroscopy of Ce^{3+} ions in dielectric fluoride crystals reveal the crystal field splitting of the 5d electronic configuration [93,163]. The luminescence spectra of Ce^{3+} in different dielectric fluoride crystal hosts consists of two bands due to transitions from the lowest Stark component of the 5d electronic configuration to the ${}^2F_{5/2}$ and ${}^2F_{7/2}$ levels of the 4f electronic configuration.

B. Praseodymium

The LIF spectrum of Pr^{3+} ions in $LiLuF_4$ single-crystal hosts [8] excited in the 4f5d electronic configuration with the F_2 molecular laser at 157 nm indicated that interconfigurational transitions mainly originate from the edge of the band of the 4f5d electronic configuration at 46400 cm^{-1} and spans the spectral range from 218 to 280 nm. Despite the fact that electron–phonon interaction within the 4f5d electronic configuration is strong, the LIF spectrum indicated the presence of two weak bands around 200 and 170 nm. These bands were assigned to interconfigurational transitions from the Stark components of the 4f5d electronic configuration at $53,200$ and $63,400\text{ cm}^{-1}$, respectively, and taking into consideration the energy gaps of the absorption spectrum (which are similar to the energy gaps in the absorption spectrum of the Tb^{3+} ions [83,135]). The two weak bands have been observed from the same crystal using x-rays as the excitation source [162]. UV fluorescence spectra using two photon excitation techniques have been recorded as well [163]. Luminescence spectra of Pr^{3+} ions in YF_3 and LaF_3 crystals, where the edge of the levels of the 4f5d electronic configuration is at $50,000\text{ cm}^{-1}$, indicated that radiative interconfigurational transitions in the UV and the visible are taking place between the 1S_0 energy level at $48,000\text{ cm}^{-1}$ and the lower energy levels of the $4f^2$ electronic configuration [24,111].

C. Neodymium

In the case of VUV excitation of the $YLF:Nd$ crystal, it was observed experimentally that the emission spectrum depends on the excitation wavelength [115]. Two

peaks in this case were situated at 181.5 and 185.3 nm. The two peaks were observed in multiphoton and single photon laser excitation of the YLF:Nd crystals as well [7,10,82], at right angle to the excitation axis. The two peaks were assigned to transitions from the low Stark component of the lower $4f^25d$ (${}^4K_{11/2}$) level of the Nd^{3+} ion to the levels of the $4f^3$ configuration.

Indeed, when the crystal field is applied on the ${}^4K_{11/2}$ level of the Nd^{3+} ion it splits it into three Stark components, $\Gamma^{(8)}$, $\Gamma^{(7)}$, and $\Gamma^{(6)}$, for a tetragonal site symmetry of the Nd^{3+} ion. The $\Gamma^{(8)}$ one is quadratic degenerate, $2(\Gamma^{(6)} + \Gamma^{(7)})$ and its degeneracy is removed when the L–S coupling is strong enough within the $4f^25d$ electronic configuration. These levels occupy the spectral range from 453 to 1700 cm^{-1} above the low energy limit of the levels of the $4f^25d$ electronic configuration, in agreement with findings by Thogersen et al. [10].

The broad band distribution of the electronic cloud near the edge of the band reflects the wide electronic character of the $4f^25d$ (${}^4K_{11/2}$) \rightarrow $4f^3$ dipole transition, with the maximum of the emission at 181.5 and 185.3 nm, respectively. The narrow emission peaks of the 180 nm band correspond to transitions from the Stark component of the $4f^25d$ (${}^4K_{11/2}$) level to the Stark components of the ${}^4I_{9/2}$, and ${}^4I_{11/2}$ levels of the $4f^3$ configuration. The ${}^4I_{9/2}$ level of the $4f^3$ configuration is split into five Stark components at 1, 139, 180, 236, and 529 cm^{-1} [82]. The ${}^4I_{11/2}$ level of the $4f^3$ configuration is split into five Stark components at 1979, 2015, 2056, 2221, and 2254 cm^{-1} . At room and low temperatures all these levels should be populated from transitions that originate from the ${}^4K_{11/2}$ electronic level of the $4f^25d$ configuration, at 55,648, 55,096, and $54,495\text{ cm}^{-1}$, respectively. In these experiments the linewidth of the $4f^25d \rightarrow 4f^3$ atomic transitions, should be less than 0.1 nm. This fact suggests that the emission cross section of the $4f^25d \rightarrow 4f^3$ transitions along the optical axis of the crystal is $\sim 10^{-15}$ – 10^{-16} cm^2 , which is two or three orders of magnitude higher than the emission cross section of the $4f^25d \rightarrow 4f^3$ transitions observed along the directions perpendicular to the optical axis of the crystal. In the later case, the linewidth of the $4f^25d \rightarrow 4f^3$ transitions was 8.5 nm [10,115], giving a value for the corresponding emission cross section of $\sim 10^{-18}\text{ cm}^2$.

A possible mechanism to explain the structure of the LIF spectrum of the 180 nm band could be phonon trapping within the levels of the Stark component of the ${}^4K_{11/2}$ level within the active volume of the crystal. This assignment is supported by the fact that the energy difference of 552 and 600 cm^{-1} between the Stark component of ${}^4K_{11/2}$ level reflects the energy difference (within the experimental error) between successive vibronic modes of the YLF:Nd lattice [82].

This process is taking place because of the efficient coupling between sites of the Nd^{3+} ions, through multipole or exchange interactions. The repopulating process of the higher vibronic modes will cease when the trapped phonons escape from the active volume by frequency shifting via the dipole-allowed $4f^25d \rightarrow 4f^3$ interconfigurational transitions.

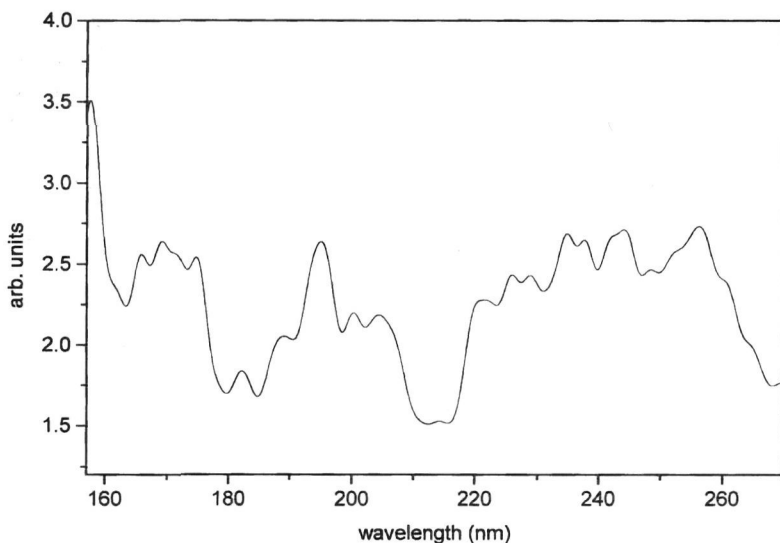


Figure 10 LIF spectrum of $\text{LiLuF}_4:\text{Tb}^{3+}$ following excitation at 157.6 nm. (From Ref. 83.)

The radiative lifetime of the transitions within the 180 nm band was found to be ~ 30 ns in agreement with previous measurements [4,6,164], using different crystal samples and measurements on VUV decay and energy transfer dynamics of Nd^{3+} ions [165] in various dielectric crystal hosts under x-ray and synchrotron excitation [166–168] for scintillation and laser [169,170] applications.

D. Terbium

Terbium trivalent ions are an interesting case since in a pure L–S coupling there is not interaction between the $4f^7$ and the $5d$ electronic configuration, the interaction is only through the crystal field. On the other hand, partial restoration of the spherical symmetry of the $5d$ electronic configuration in the crystal field of the surrounding ligands is taking place. The LIF spectrum in the spectral range from 150 to 270 nm under excitation at 157.6 nm, with the F_2 laser, for 0.01 at.% concentration of the Tb^{3+} ion at liquid nitrogen temperature, is in Figure 10. The fluorescence peaks were assigned to the dipole transitions between the levels of the $4f^7 5d$ electronic configuration and the levels of the $4f^8$ electronic configuration of the Tb^{3+} ion [83]. When the Tb^{3+} ion is excited from its $4f^8$ (${}^7\text{F}_6$) ground level to a given level of the $4f^7 5d$ electronic configuration, the experimental evidences indicate that it populates the levels of the $4f^8$ electronic configuration,

from both the levels and the edge of the $4f^{75}d$ electronic configuration. Direct emission from the levels of the $4f^{75}d$ electronic configuration could take place only when two successive electronic levels are well separated by the combined energy of few phonons, as mentioned previously. However, according to Szczurek and Schlesinger [81], there are 3106 electronic levels of the $4f^{75}d$ electronic configuration in the energy range from 80,000 to 45,000 cm^{-1} . This number corresponds to the energy level density of 13 electronic levels per wavenumber (considering an even distribution of the energy levels over the spectral range). Hence there is a small probability of direct transitions between the Stark components of the levels of the $4f^{75}d$ electronic configuration and the levels of the $4f^8$ electronic configuration. Therefore the LIF spectrum can be interpreted provided that repopulation of the levels of the $4f^{75}d$ electronic configuration is taking place. The repopulation occurs via phonon reabsorption and trapping within the levels of the $4f^{75}d$ electronic configuration. These kind of processes have their origin in the strong ionic coupling between two different Tb^{3+} ions through multipole or exchange interactions, and they have been observed previously for different crystal samples as well [172]. The repopulating process will cease when the trapped phonons escape from the active volume by frequency shifting via the interconfigurational transitions. Phonon trapping is usually detected by observing the fluorescent radiation from the excited levels to the ground state. In the case of weak electron [$4f^{n-1}$]-phonon interaction and/or spin-forbidden $4f^{n-1}5d$ transitions, the phonon trapping and reabsorption processes compete with the nonradiative relaxation process within the levels of the $4f^{n-1}5d$ electronic configuration. In this case, the interconfigurational transitions from inside the levels of the $4f^{n-1}5d$ electronic configuration are strong enough, as for example in the case of the Tb^{3+} , Gd^{3+} , and Er^{3+} ions [172]. In the case of strong electron-phonon interaction, for example for the Nd^{3+} ion, the rate of the internal relaxation within the levels of the $4f^{n-1}5d$ electronic configuration is higher than the rate of the phonon reabsorption within the levels of the $4f^{n-1}5d$ electronic configuration. In this case, the dipole transitions originate mainly from the edge of the levels of the $4f^{n-1}5d$ electronic configuration.

As one finds from the LIF spectrum in Figure 10, the dipole transitions, between the 7D_5 Stark components of the $4f^{75}d$ electronic configuration and the levels of the $4f^8$ electronic configuration are due to the dipole transitions ${}^7D_5 \rightarrow {}^7F_{4,5,6}$, which satisfy the selection rules for electric dipole transitions $\Delta S = 0$, $\Delta l = +1, -1$, $\Delta L = 0, +1, -1$, $\Delta J = 0, +1, -1$ and $\Delta J = \Delta L$.

The emission band, which covers the spectral range from 220 to 253 nm, reflects the wide electronic character of the $4f^{75}d({}^7D_5) \rightarrow 4f^8({}^7F_{0-6})$ dipole transitions of the Γ_4 Stark component of the levels of the $4f^{75}d({}^7D_5)$ electronic configuration. The interconfigurational transitions in this spectral range originate from the edge of the levels of the $4f^{75}d$ electronic configuration. From the LIF spectrum of [83], it was found that the energy position with the higher Frank-Condon

factor is at $(45.2 \pm 0.2) \times 10^3 \text{ cm}^{-1}$. In this case the following assignments can be made regarding the observed dipole transitions (Fig. 11).

$$4f^7 5d[{}^7D_5(\Gamma_4), 45.2 \times 10^3 \text{ cm}^{-1}] \rightarrow 4f^8({}^7F_6, 0) + h\nu(221.2 \text{ nm})$$

$$4f^7 5d[{}^7D_5(\Gamma_4), 45.2 \times 10^3 \text{ cm}^{-1}] \rightarrow 4f^8({}^7F_5, 1.5 \times 10^3 \text{ cm}^{-1}) + h\nu(228.8 \text{ nm})$$

$$4f^7 5d[{}^7D_5(\Gamma_4), 45.2 \times 10^3 \text{ cm}^{-1}] \rightarrow 4f^8({}^7F_4, 3.1 \times 10^3 \text{ cm}^{-1}) + h\nu(237.7 \text{ nm})$$

Besides the above-observed dipole-allowed transitions, dipole-forbidden transitions [173] ($\Delta J \neq 0, \pm 1$) were observed from the Γ_4 Stark component of the levels of the $4f^7 5d({}^7D_5)$ electronic configuration.

$$4f^7 5d[{}^7D_5(\Gamma_4), 45.2 \times 10^3 \text{ cm}^{-1}] \rightarrow 4f^8({}^7F_3, 4.0 \times 10^3 \text{ cm}^{-1}) + h\nu(242.5 \text{ nm})$$

$$4f^7 5d[{}^7D_5(\Gamma_4), 45.2 \times 10^3 \text{ cm}^{-1}] \rightarrow 4f^8({}^7F_2, 4.2 \times 10^3 \text{ cm}^{-1}) + h\nu(244.2 \text{ nm})$$

$$4f^7 5d[{}^7D_5(\Gamma_4), 45.2 \times 10^3 \text{ cm}^{-1}] \rightarrow 4f^8({}^7F_1, 5.0 \times 10^3 \text{ cm}^{-1}) + h\nu(248.5 \text{ nm})$$

$$4f^7 5d[{}^7D_5(\Gamma_4), 45.2 \times 10^3 \text{ cm}^{-1}] \rightarrow 4f^8({}^7F_0, 5.6 \times 10^3 \text{ cm}^{-1}) + h\nu(252.7 \text{ nm})$$

The position of the levels of the $4f^8$ electronic configuration of the Tb^{3+} ion in the LiLuF_4 , single-crystal host, is not known exactly. The position of these levels in the free ion case, for the ${}^7F_{0-5}$ terms is at 58,000, 51,000, 48,000, 40,000, 31,000, and 19,000 cm^{-1} respectively. From the LIF spectrum and for the Γ_4 Stark component, the experimental position of the ${}^7F_{0-5}$ terms in the LiLuF_4 crystal was found to be at 56,000, 50,000, 42,000, 40,000, 31,000, and 15,000 cm^{-1} , respectively. Taking into consideration the fact that the electrons of the $4f^8$ electronic configuration are well screened by the electrons of the $5d$ electronic configuration, the position of the levels of the $4f^8$ electronic configuration inside the LiLuF_4 crystal should be shifted relative to the position of the levels in the free ion case, by few wavenumbers, and this situation is reflected well in the experimental data.

The emission spectrum that covers the spectral region from 193 to 220 nm can likewise be assigned to the dipole transitions between the Γ_5 Stark component of the $4f^7 5d({}^7D_5)$ electronic configuration, with maximum of absorption at 54,400 cm^{-1} and the levels of the $4f^8$ electronic configuration. In this case the Frank–Condon factor of the corresponding transitions has its highest value at $(52.9 \pm 0.2) \times 10^3 \text{ cm}^{-1}$. For these transitions, the following assignments can be made within the limits of the experimental error of 200 cm^{-1} for these wavelengths.

$$4f^7 5d[{}^7D_5(\Gamma_5), 52.9 \times 10^3 \text{ cm}^{-1}] \rightarrow 4f^8({}^7F_6) + h\nu(188.9 \text{ nm})$$

$$4f^7 5d[{}^7D_5(\Gamma_5), 52.9 \times 10^3 \text{ cm}^{-1}] \rightarrow 4f^8({}^7F_5, 1.5 \times 10^3 \text{ cm}^{-1}) + h\nu(194.7 \text{ nm})$$

$$4f^7 5d[{}^7D_5(\Gamma_5), 52.9 \times 10^3 \text{ cm}^{-1}] \rightarrow 4f^8({}^7F_4, 3.0 \times 10^3 \text{ cm}^{-1}) + h\nu(200.2 \text{ nm})$$

$$4f^7 5d[{}^7D_5(\Gamma_5), 52.9 \times 10^3 \text{ cm}^{-1}] \rightarrow 4f^8({}^7F_3, 4.0 \times 10^3 \text{ cm}^{-1}) + h\nu(204.5 \text{ nm})$$

From the LIF spectrum [83], it was found that the position of the Stark components of the levels of the $4f^8$ electronic configuration ${}^7F_{3-5}$ in the LiLuF_4 crystal

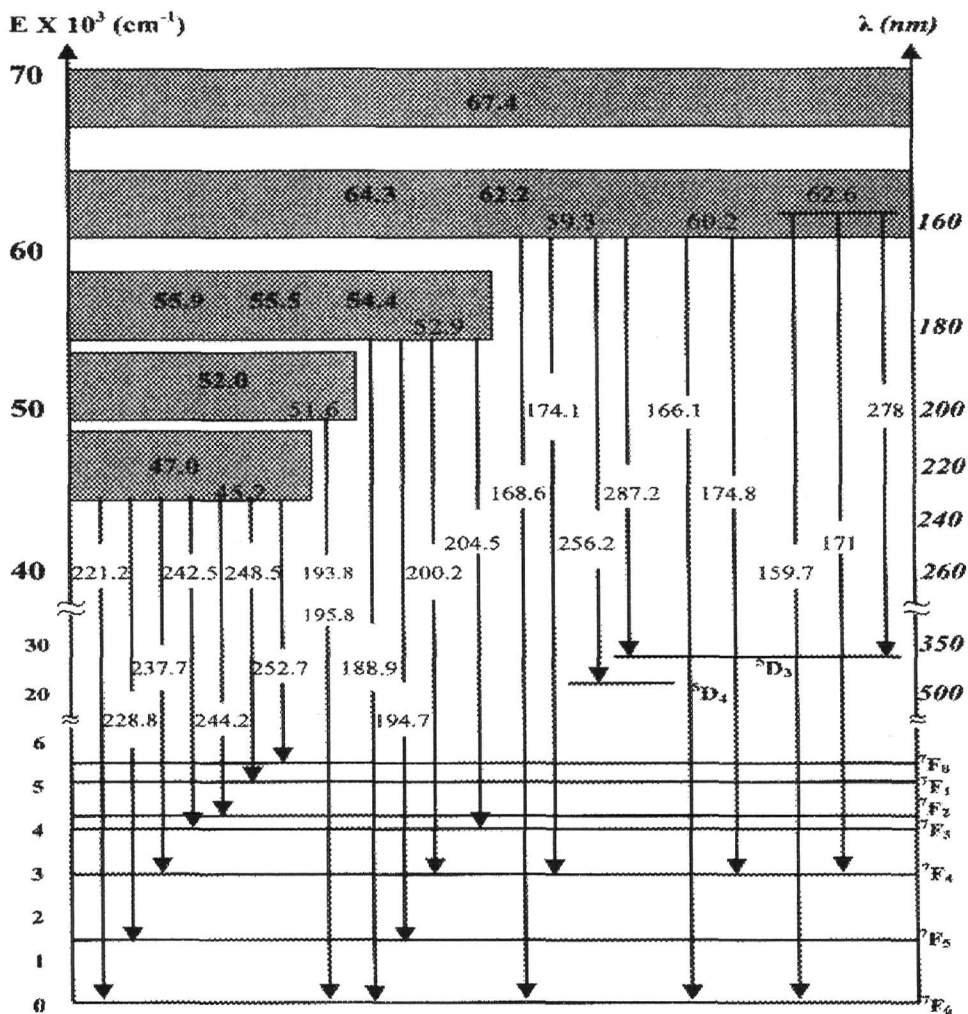


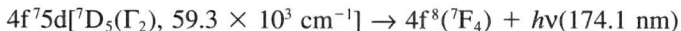
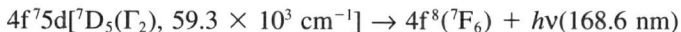
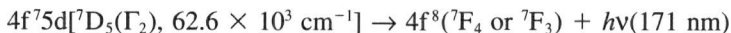
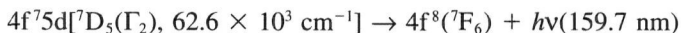
Figure 11 Simplified energy diagram shows various transitions of the LIF spectra of the $LiLuF_4:Tb^{3+}$ crystal. The position of levels of the $4f^75d$ electronic configuration of the Tb^{3+} ion is where the maximum absorption is taking place.

is at 40,000, 30,000, and 15,000 cm^{-1} , respectively, in agreement with the energy position of these levels in the spectral range from 220 to 253 nm.

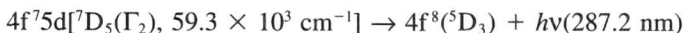
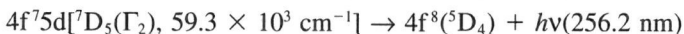
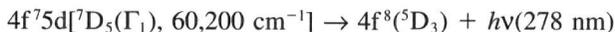
The transition around 194 nm could originate as well from the Γ_3 Stark component, with maximum of absorption at 52,000 at 51,600 cm^{-1} .



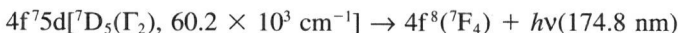
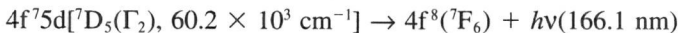
The emission spectrum, which covers the spectral range from 159 to 174 nm, can be assigned to the dipole transitions between the Γ_2 Stark component of the $4f^75d({}^7D_5)$ electronic configuration, and the levels of the $4f^8$ electronic configuration. However, for this spectral range, it is difficult to make any specific assignment for the $4f^75d \rightarrow 4f^8$ transitions, due to the presence of intense scattered laser light. Taking into consideration the position of the levels of the Tb^{3+} ions of the $4f^8$ electronic configuration in the LiLuF_4 crystal host, and the emission spectrum, the following assignments can be made for the $4f^75d \rightarrow 4f^8$ transitions:



The transitions at 278, 256.2, and 287.2 nm were assigned to the spin-forbidden transitions [173], taking into consideration that the energy position of the 5D_4 and 5D_3 levels of the $4f^8$ electronic configuration in the free Tb^{3+} ion case is at 20,500 and 26,000 cm^{-1} , respectively.



The transitions at 166.1 and 174.8 nm [83] can be assigned to the interconfigurational transitions originating from the energy position at 60,200 cm^{-1} .



E. Holmium

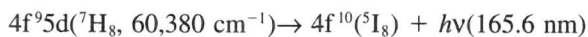
The LIF spectrum of the $\text{LiYF}_4:\text{Ho}^{3+}$ crystal, under excitation at 157.6 nm with the F_2 laser, for 0.1 at.% concentration of the Ho^{3+} ion at liquid nitrogen temperature includes both spin-allowed and spin-forbidden interconfigurational transitions and intraconfigurational transitions [7,174,175]. The emission peak at 171.2 nm is assigned to the interconfigurational spin-allowed transition from the lower

Stark component of the 5H_7 term at $63,450\text{ cm}^{-1}$ (157.6 nm) to the 5I_7 level of the $4f^{10}$ electronic configuration:



The spin-allowed transition to the ground 5I_8 level (which is expected at 157.6 nm) was not observed due to the presence of the intense laser scattered light.

The lowest 7H_8 level of the $4f^9 5d$ electronic configuration should likewise split into four doubly degenerate Stark components in the LiYF_4 crystal field. The transitions that originate from the Stark components of the $4f^9 5d$ (7H_8) electronic configuration are spin-forbidden and therefore they are expected to be of low intensity. The transitions at 167.5 and 165.6 nm are assigned to the spin-forbidden transitions as follows:



The LIF transitions from 172.5 to 189 nm were assigned to the $4f^{10} \rightarrow 4f^{10}$ intraconfigurational transitions. From both emission and absorption spectra, the dipole-forbidden transitions at 172.5, 174, 177.5, 178.5, 181, 185, 188, and 189 nm were assigned to the transitions from the high excited levels of the $4f^{10}$ electronic configuration to the ground 5I_8 level [174,175].

F. Erbium

The LIF spectrum of the Er^{3+} ions in LiYF_4 crystal hosts of Figure 12 includes both spin-allowed and spin-forbidden transitions. The emission bands at 158.6, 157, and 195 nm were assigned to dipole-allowed transitions from the edge of the lower energy level of the $4f^{10} 5d$ electronic configuration to the energy levels of the $4f^{11}$ electronic configuration [9]. Emission at 167–169 nm from an absorption band situated at 163 nm [115] was observed for the first time by Sarantopoulou et al. [9]. It was assigned to spin-forbidden transitions from the Stark component of the $4f^{11}$ electronic configuration to the ground level $^4I_{15/2}$ of the $4f^{11}$ electronic configuration [9,150]. VUV emission of Er^{3+} ions in various dielectric hosts using synchrotron and x-ray excitation has been reported as well [176–179].

G. Thulium

Due to the fact that the laser photons at 157 nm populate the $4f^{11} 5d$ electronic configuration of the Tm^{3+} ions in LiLuF_4 crystal hosts just above the edge of the band [135], the LIF spectrum of the $\text{LiYF}_4:\text{Tm}^{3+}$ monocrystals, under the F_2 laser excitation, exhibits strong interconfigurational transitions in the VUV (Fig. 13).

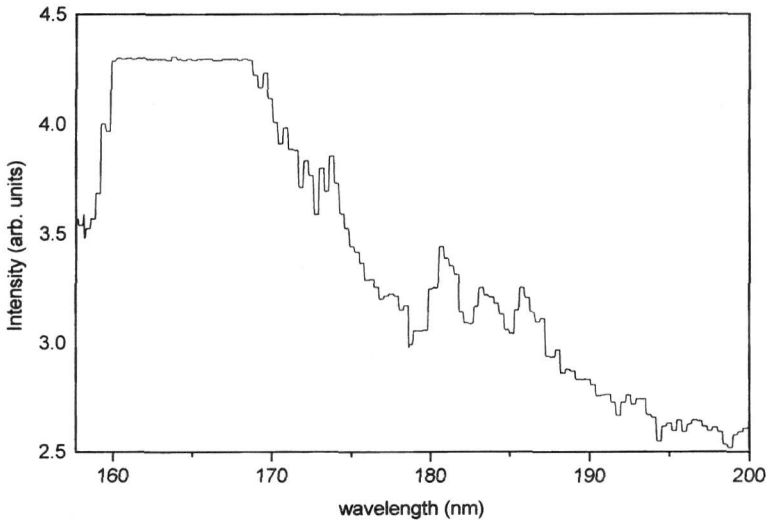


Figure 12 VUV LIF spectrum of LiLuF₄:Er³⁺ crystal under F₂ laser excitation.

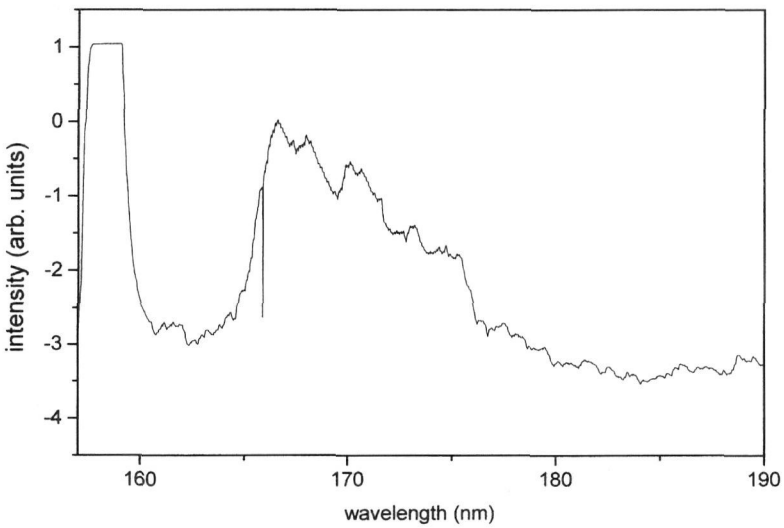


Figure 13 VUV LIF spectrum of LiYF₄:Tm³⁺ crystals under F₂ laser excitation.

REFERENCES

1. KH Yang, JA DeLuka. VUV fluorescence of Nd^{3+} , Er^{3+} and Tm^{3+} and Tm^{3+} doped trifluorides and tuneable coherent sources from 1650 to 2600 nm. *Appl Phys Lett* 29: 499–501, 1976.
2. S Heaps, LR Elias, WM Yen. Vacuum-ultraviolet bands of trivalent lanthanides in LaF_3 . *Phys Rev B* 13: 94–104, 1976.
3. KH Yang, JA DeLuca. Vacuum ultraviolet excitation studies of $5d^1 4f^{n-1}$ to $4f^n$ and $4f^n$ to $4f^n$ transitions of Nd^{3+} , Er^{3+} and Tm^{3+} -doped trifluorides. *Phys Rev B* 17: 4246–4255, 1978.
4. MA Dubinskii, AC Cefalas, E Sarantopoulou, RY Abdulsabirov, SL Korableva, AK Naumov, VV Semashko. On the interconfigurational $4f^2 5d$ – $4f^3$ VUV and UV fluorescence features of Nd^{3+} in YLF single crystals under fluorine laser pumping. *Opt Commun* 94: 115–118, 1992.
5. JP Krupa, I Gerard, A Mayoler, P Martin. Electronic structure of f-element system in the UV and VUV energy range. *Acta Phys Pol A84*: 843–848, 1993.
6. R Visser, P Dorenbos, CWE Van Eijk, A Meijerink, HW den Hartog. The scintillation intensity and decay from $\text{Nd}^{3+} 4f^2 5d$ and $4f^3$ excited states in several fluoride crystals. *Phys Cond Matt* 5: 8437–8460, 1993.
7. E Sarantopoulou, AC Cefalas, MA Dubinskii, CA Nicolaidis, RY Abdulsabirov, SL Korableva, AK Naumov, VV Semashko. VUV and UV fluorescence and absorption studies of Nd^{3+} and Ho^{3+} ions in LiYF_4 single crystals. *Opt Commun* 107: 104–110, 1994.
8. E Sarantopoulou, AC Cefalas, MA Dubinskii, CA Nicolaidis, RY Abdulsabirov, SL Korableva, AK Naumov, VV Semashko. VUV and UV fluorescence and absorption studies of Pr^{3+} -doped LiLuF_4 single crystals. *Opt Lett* 19: 499–501, 1994.
9. E Sarantopoulou, Z Kollia, AC Cefalas, MA Dubinskii, CA Nicolaidis, RY Abdulsabirov, SL Korableva, AK Naumov, VV Semashko. Vacuum ultraviolet and ultraviolet fluorescence and absorption studies of Er^{3+} -doped LiLuF_4 single crystals. *Appl Phys Lett* 65: 813–815, 1994.
10. J Thogersen, JD Gill, HK Haugen. Stepwise multiphoton excitation of the $4f^2 5d$ configuration in Nd^{3+} :YLF. *Opt Commun* 132: 83–88, 1996.
11. S Guy, MF Joubert, B Jacquier. Photon avalanche and mean-field approximation. *Phys Rev B* 55: 8240–8248, 1997.
12. M Malinowski, B Jacquier, M Bouazaoui, MF Joubert, C Linares. Laser induced fluorescence and up conversion processes in LiLuF_4 : Nd^{3+} laser crystals. *Phys Rev B* 41: 31–40, 1990.
13. DJ Ehrlich, PF Moulton, RM Osgood Jr. Ultraviolet solid state Ce:YLF laser at 325 nm. *Opt Lett* 4: 184–186, 1979.
14. K-S Lim, DS Hamilton. Optical gain and loss studies in Ce^{3+} : YLiF_4 . *J Opt Soc Am B6*: 1401–1406, 1989.
15. DJ Ehrlich, PF Moulton, RM Osgood Jr. Optically pumped Ce: LaF_3 laser at 286 nm. *Opt Lett* 5: 339–341, 1980.
16. RW Waynant, PH Klein. Vacuum ultraviolet emission from Nd^{3+} : LaF_3 . *Appl Phys Lett* 46: 14–15, 1985.
17. RW Waynant. Vacuum ultraviolet laser emission from Nd^{3+} : LaF_3 . *Appl Phys B* 28: 205, 1982.

18. MA Dubinskii, AC Cefalas, CA Nicolaidis. Solid state Nd^{3+} doped LaF_3 VUV laser pumped by a pulsed discharge fluorine-molecular laser at 157 nm. *Opt Commun* 88: 122–124, 1992.
19. JC van't Spijker, P Dorenbos, CWE van Eijk, JEM Jacobs, HW den Hartog, N Korolev. Luminescence and scintillation properties of $\text{BaY}_2\text{F}_8:\text{Ce}^{3+}$, BaLu_2F_8 and $\text{BaLu}_2\text{F}_8:\text{Ce}^{3+}$. *J Lumin* 85: 11–19, 1999.
20. S Kubodera, M Kitahara, J Kawanaka, W Sasaki, K Kurosawa. A vacuum ultraviolet flash lamp with extremely broadened emission spectra. *Appl Phys Lett* 69: 452–454, 1996.
21. G Blasse, BC Grabmayer. *Luminescent Materials*. Berlin: Springer Verlag, 1996.
22. RT Wegh, H Donker, A Meijerink, RJ Lamminmaki, J Holsa. Vacuum-ultraviolet spectroscopy and quantum cutting for Gd^{3+} in LiLuF_4 . *Phys Rev B* 56: 13841–13848, 1997.
23. CM Combes, P Dorenbos, CWE Vaneijk, C Pedrini, HW Denhartog, JY Gesland, PA Rodnyi. Optical and scintillation properties of Ce^{3+} doped LiYF_4 and LiLuF_4 crystals. *J Lumin* 71: 65–70, 1997.
24. AM Srivastava, SJ Duclos. On the luminescence of $\text{YF}_3\text{-Pr}^{3+}$ under vacuum ultraviolet and X-ray emission. *Chem Phys Lett* 275: 453–456, 1997.
25. MJF Dignonnet, RW Sadowski, HJ Shaw, RH Pantell. Resonantly enhanced nonlinearity in doped fibers for low power all optical switching. *Opt Fib Techn* 3: 44–64, 1997.
26. CD Marshall, JA Speth, SA Payne, WF Krupke, GJ Quarles, V Castillo, B Chai. Ultraviolet laser emission properties of Ce^{3+} doped LiSrAlF_6 and LiCaAlF_6 . *J Opt Soc Am B* 11: 2054–2065, 1994.
27. TM Bloomstein, M Rothschild, RR Kunz, DE Hardy, RB Goodman, ST Palmacci. Critical issues in 157 nm lithography. *J Vac Sci Techn B* 16: 3154–3157, 1998.
28. AC Cefalas, E Sarantopoulou, P Argitis, E Gogolides. Mass spectroscopic and degassing characteristics of polymeric materials for 157 nm photolithography. *Appl Phys A* 69: 5229–5234, 2000.
- 28a. E Sarantopoulou, Z Kollia, AC Cefalas. $\text{YF}_3:\text{Nd}^{3+}$, Pr^{3+} , Gd^{3+} wide band gap crystals as optical materials for 157 nm photolithography. *Optical Materials* 18: 23–26, 2001.
29. GH Dieke, HM Crosswhite. The spectra of the doubly and triply ionized rare earths. *Appl Opt* 2: 675–686, 1963.
30. R Hilbic, R Wallenstein. Enhanced Production of Tunable VUV Radiation by phase-matched frequency tripling in krypton and xenon. *IEEE J Quantum Electron* 17: 1566–1573, 1981.
31. W Jamroz, PE LaRocque, BP Stoicheff. Generation of continuously tunable coherent vacuum-ultraviolet radiation (140–106 nm) in zinc vapor. *Opt Lett* 7: 617–619, 1982.
32. JC Miller, RN Compton, CD Cooper. Vacuum ultraviolet spectroscopy of molecules using third-harmonic generation in rare-gases. *J Chem Phys* 76: 3967–3973, 1982.
33. Y Hirakawa, K Nakai, T Obara, M Maeda, K Muraoka. Generation of coherent

- XUV radiation by 2-photon resonant 4-wave-mixing combined with stimulated Raman-scattering. *Opt Commun* 92: 215–218, 1992.
34. K Miyazaki, H Sakai, T Sato. Efficient deep-ultraviolet generation by frequency doubling in beta-BaB₂O₄ crystals. *Opt Lett* 11: 797–799, 1986.
 35. BC Wu, F Xie, C Chen, D Deng, Z Xu. Generation of tunable coherent vacuum ultraviolet-radiation in LiB₃O₅ crystal. *Opt Commun* 88: 451–454, 1992.
 36. NG Basov, VA Danilychev. Condensed- and compressed-gas lasers. *Sov Phys Usp* 29:31–56, 1986.
 37. RH Lipson, PE Larocque, BP Stoicheff. Vacuum ultraviolet laser-excited spectra of Xe₂. *Opt Lett* 9: 402–404, 1984.
 38. T Eftimiopoulos, BP Stoicheff, RI Thomson. Efficient population-inversion in excimer states by supersonic expansion of discharge plasmas. *Opt Lett* 14: 624–626, 1989.
 39. H Nahme, N Schwentner. Luminescence of rare-gas crystals at high-excitation densities for VUV laser applications. *Appl Phys B* 51: 177–191, 1990.
 40. AC Cefalas, TA King. Injection locking of ArF excimer lasers. *Appl Phys B* 37: 159–164, 1985.
 41. AC Cefalas, TA King. Phase conjugation by four wave mixing in an ArF excimer amplifier. *Opt Commun* 51: 105–110, 1984.
 42. JR Woodworth, JK Rice. An efficient high-power F₂ laser near 157 nm. *J Chem Phys* 69: 2500–2504, 1978.
 43. JR Woodworth, JK Rice. High intensity laser photolysis of OCS at 157 nm. *IEEE J Quantum Electron* 15: 88D–89D, 1979.
 44. H Pummer, OK Hohla, M Digelman, JP Reilly. Discharge pumped F₂ pulsed laser at 1580 Å. *Opt Commun* 28: 104–106, 1979.
 45. AC Cefalas, C Skordoulis, M Kompitsas, CA Nikolaidis. Gain measurements at 157 nm in an F₂ pulsed discharge molecular laser. *Opt Commun* 55: 423–426, 1985.
 46. VN Ishchenko, SA Kochubei, AM Razhev. High-power efficient vacuum ultraviolet F₂ laser excited by an electric discharge. *Sov J Quantum Electron* 16:707–709, 1986.
 47. M Ohwa, M Obara. Theoretical evaluation of high-efficiency operation of discharge-pumped vacuum ultraviolet F₂ lasers. *Appl Phys Lett* 51: 958–960, 1987.
 48. K Yamada, K Miyazaki, T Hasama, T Sato. High-power discharge-pumped F₂ molecular laser. *Appl Phys Lett* 54: 597–599, 1989.
 49. C Skordoulis, E Sarantopoulou, S Spyrou, AC Cefalas. Amplification characteristics of a discharge excited F₂ laser. *J Mod Opt* 37: 501–509, 1990.
 50. C Skordoulis, S Spyrou, AC Cefalas. Gain and saturation measurements in a discharge excited F₂ laser using an oscillator amplifier configuration. *Appl Phys B* 51: 141–145, 1990.
 51. H Nishimura, DC Cartwright, J Trajmar. Electron energy loss spectroscopy of molecular fluorine. *J Chem Phys* 71: 5039–5041, 1979.
 52. DJ Cartwright, PJ Hay. Theoretical studies of the valence electronic states and the ${}^1\Pi_u \rightarrow X\ {}^1\Sigma_g^+$ absorption spectrum of the F₂ molecule. *J Chem Phys* 70: 3191–3203, 1979.

53. K Hoshiba, Y Fujita, SS Kano, H Takuma, T Takayanagi, K Wakiya, H Suzuki. Experimental observation of the F_2 VUV laser levels. *J Phys B Atom Mol Phys* 18: L875–L879, 1985.
54. RG Wang, ZW Wang, MA Dillon, D Spense. Electron energy loss spectroscopy of molecular fluorine. *J Chem Phys* 80: 3574–3579, 1984.
55. AC Cefalas, TA King. A doubly preionized ArF laser. *J Phys E: Sci Instr* 17: 760–764, 1984.
56. RC Caro, MC Gower, CE Webb. A simple tunable KrF laser system with narrow bandwidth and diffraction limited divergence. *J Phys D Appl Phys* 15: 767–773, 1982.
57. R Loudon. *The Quantum Theory of Light*. Oxford: Oxford University Press, 1973.
58. NN Ershov, NG Zakharov, PA Rodnyi. Spectral-kinetic study of the intrinsic luminescence characteristics of a fluorite-type crystal. *Opt Spectrosk* 53: 51–54, 1982.
59. CWE van Eijk. Cross-luminescence. *J Lumin* 60: 936–941, 1994.
60. E Sarantopoulou, Z Kollia, AC Cefalas. $LiCaAlF_6:Nd^{3+}$ crystal as optical material for 157 nm photolithography. *Opt Commun* 177: 377–382, 2000.
61. Z Kollia, E Sarantopoulou, AC Cefalas, CA Nikolaidis, AK Naumov, VV Semashko, RYu Abdulsabirov, SL Korableva, MA Dubinskii. Vacuum-ultraviolet inter-configurational $4f^3 \rightarrow 4f^25d$ absorption and emission studies of the Nd^{3+} ion in KYF, YF and YLF crystal hosts. *J Opt Soc Am B* 12: 782–785, 1995.
62. V Dauer. Optical constants of lithium fluoride thin films in the far ultraviolet. *J Opt Soc Am B* 17: 300–303, 2000.
63. ED Palik, ed. *Handbook of Optical Constants of Solids*. 1st ed. Orlando, FL: Academic Press, 1985.
64. A Milgram, M Parker Givens. Extreme ultraviolet absorption by lithium fluoride. *Phys Rev* 125: 1506–1509, 1962.
65. P Laporte, JL Subtil, M Courbon, M. Bon. Vacuum ultraviolet refractive index of LiF and MgF_2 in the temperature range 80–300K. *J Opt Soc Am* 73: 1062–1069, 1983.
66. G Stephan, YLe Calvez, JC Lemonier, Mme S Robin. Propriétés optiques et spectre électronique du MgF_2 et du CaF_2 de 10 à 48 eV. *J Phys Chem Solids* 30: 601–608, 1969.
67. OR Wood, HG Craighead, JE Sweeney, PJ Maloney. Vacuum ultraviolet loss in magnesium fluoride films. *Appl Opt* 23: 3644–3649, 1984.
68. MW Williams, RA MacRae, ET Arakawa. Optical properties of magnesium fluoride in the vacuum ultraviolet. *J Appl Phys* 38: 1701–1705, 1966.
69. ET Hutcheson, G Hass, JT Cox. Effect of deposition rate and substrate temperature on the vacuum ultraviolet reflectance of MgF_2 - and LiF-overcoated aluminum mirrors. *Appl Opt* 11: 2245–2248, 1972.
70. AS Barriere, A Lachter. Optical transitions in disordered thin films of the ionic compounds MgF_2 and AlF_3 as a function of their conditions of preparation. *Appl Opt* 16: 2865–2871, 1977.
71. A Mayolet, JC Krupa, I. Gerard, P. Martin. Luminescence of Eu^{3+} doped materials excited by VUV synchrotron radiation. *Materials Chem Phys* 31: 107–109, 1992.
72. AN Belsky, JC Krupa. Luminescence excitation mechanisms of rare earth doped phosphors in the VUV range. *Displays* 19:185–196, 1999.

73. G Ionova, JC Krupa, I. Gerard, R. Guillaumont. Systematics in electron-transfer energies for lanthanides and actinides. *N J Chem* 19: 677–689, 1995.
74. I Gerard, JC Krupa, E Simoni, P Martin. Investigation of charge transfer $O^{2-} \rightarrow Ln^{3+}$ and $F^- \rightarrow Ln^{3+}$ in $LaF_3: (Ln^{3+}, O^{2-})$ and $YF_3: (Ln^{3+}, O^{2-})$ systems. *J Alloys Comp* 207/208: 120–127, 1994.
75. HR Moser, G Wendin. Theoretical-models for intensities of d-f transitions in electron-energy-loss spectra of rare-earth and actinide metals. *Phys Rev B* 44: 6044–6061, 1991.
76. BF Aull, HP Jenssen. Impact of ion-host interactions on the 5d to 4f spectra of lanthanide rare-earth-metal ions. I. A phenomenological crystal field model. *Phys Rev B* 34: 6640–6646, 1986.
77. L Brewer. Energies of the electronic configurations of the singly, doubly and triply ionized lanthanides and actinides. *J Opt Soc Am* 61: 1666–1682, 1971.
78. BR Judd. Optical absorption intensities of rare-earth ions. *Phys Rev B* 127: 750–761, 1962.
79. E Loh. $4f^n \rightarrow 4f^{n-1}5d$ spectra of rare earth ions in crystals. *Phys Rev B* 175: 533–536, 1968.
80. NV Starostin. On the theory of composite $f^{n-1}d$ configuration of lanthanides in crystalline fields of cubic symmetry. *Opt Spec* 23: 260–261, 1964.
81. T Szcurek, M Schlesinger. Vacuum ultraviolet absorption spectra of $CaF_2:RE^{3+}$ crystals. In: *Proceedings of the International Symposium Rare Earth Spectroscopy*. Singapore: World Scientific, pp 309–330, 1985.
82. Z Kollia, E Sarantopoulou, AC Cefalas, AK Naumov, VV Semashko, RYu Abdulsabirov, SL Korableva. On the $4f^25d \rightarrow 4f^3$ interconfigurational transitions of Nd^{3+} ions in K_2YF_5 and $LiYF_4$ crystal hosts. *Opt Commun* 149: 386–392, 1998.
83. E Sarantopoulou, Z Kollia, AC Cefalas, VV Semashko, R Yu Abdulsabirov, AK Naumov, SL Korableva. On the VUV and UV $4f^7(^8S)5d \rightarrow 4f^3$ interconfigurational transitions of Tb^{3+} ions in $LiLuF_4$ single crystal hosts, *Opt Commun* 156: 101–111, 1998.
84. P Feofilov. On absorption and luminescence spectra of Ce^{3+} ions. *Opt Spectr* 6: 150–151, 1959.
85. AA Kaplyanski, VN Medvedev, PP Feofilov. The spectra of trivalent cerium ions in alkaline earth fluoride crystals. *Opt Spect* 14: 351–356, 1963.
86. MH Crozier. Zeeman effect in the $4f \rightarrow 5d$ spectrum of Ce^{3+} in CaF_2 . *Phys Rev* 137: A1781–A1783, 1965.
87. AA Kaplyanski, VN Medvedev. Piezospectroscopic determination of the symmetry of the crystal field acting on trivalent ions of rare-earth in fluorite lattice. *Opt Spect* 18: 451–456, 1965.
88. AA Kaplyanski, VN Medvedev. Linear Stark effect in the spectra of local centers in cubic crystals. *Opt Spect* 23: 404–410, 1967.
89. SK Gayen, DS Hamilton. Two photon excitation of the lowest 4f-5d near ultraviolet transition in $Ce^{3+}: CaF_2$. *Phys Rev B* 28: 3706–3711, 1983.
90. MA Dubinskii, VV Semashko, AK Naumov, R Yu Abdulsabirov, SL Korableva. Spectroscopy of new active medium of a solid-state UV laser with broadband single pass gain. *Laser Phys* 3: 216–217, 1993.
91. IT Jacobs, GD Jones, K Zdansky, RA Satten. Electron phonon interaction of hydro-

- genated, deuterogenated and tritiated crystals of calcium and strontium fluoride containing cerium. *Phys Rev B* 3: 2888–2910, 1971.
92. E Loh. Lowest 4f-5d transition of trivalent rare-earth ions in CaF_2 crystals. *Phys Rev* 147: 332–335, 1966.
 93. M Yamaga, D Lee, B Henderson, T Han, H Gallagher, T Yosida. The magnetic and optical properties of Ce^{3+} in LiLuCaAlF_6 . *J Phys Cond. Matter* 10: 3223–3237, 1998.
 94. CD Marshall, JA Speth, SA Payne, WF Krupke, GJ Quarles, V Castillo. Ultraviolet laser emission properties of Ce^{3+} -doped LiSrAlF_6 and LiCaAlF_6 . *J Opt Soc Am B* 11: 2054–2065, 1994.
 95. E Loh. Ultraviolet absorption spectra of Ce^{3+} ion in alkaline-earth fluorides. *Phys Rev* 154: 270–276, 1967.
 96. WJ Manthey. Ultraviolet absorption spectra of Ce^{3+} ion in alkaline-earth fluorides. *Phys Rev B* 8: 4086–4098, 1973.
 97. E Loh, G Samoggia, E Reguzzoni, L Nosenzo. Thermally modulated ultraviolet absorption spectra of $\text{CaF}_2:\text{Ce}^{3+}$ crystals. *Phys Status Solidi B* 79: 795–799 (1977).
 98. M Schlesinger, PW Whipple. Investigations of 4f-5d transitions of Ce^{3+} in CaF_2 . *Phys Rev* 171: 361–364, 1968.
 99. T Szczurek, GWF Drake, M Schlesinger. Vibronic structure in the absorption spectrum of the Ce^{3+} ion in CaF_2 . *Phys Rev B* 8: 4910–4912, 1973.
 100. J Sugar. Analysis of the spectrum of triply ionized praseodymium (Pr IV). *J Opt Soc Am* 55: 1058–1061, 1965.
 101. GH Dieke, HM Crosswhite, B Dunn. Emission spectra of the doubly and triply ionized rare earths. *J Opt Soc Am* 51: 820–827, 1961.
 102. R Sarup, M Crozier. Analysis of the eigenstates of Pr^{3+} in LaCl_3 using the Zeeman effect in high fields. *J Chem Phys* 42: 371–376, 1965.
 103. J Sugar. Description and analysis of the third spectrum of cerium. *J Opt Soc Am* 55: 33–58, 1965.
 104. E Loh. $^1\text{S}_0$ level of Pr^{3+} in crystals of fluorides. *Phys Rev A* 140: 1463–1466, 1965.
 105. WT Carnall, PR Fields, R Sarup. $^1\text{S}_0$ level of Pr^{3+} in crystal matrices and energy-level parameters for the $4f^2$ configuration of Pr^{3+} in LaF_3 . *J Chem Phys* 51: 2587–2591, 1969.
 106. EY Wong, OM Stafsudd, DR Johnston. Absorption and fluorescence spectra of several praseodymium-doped crystals and the change of covalence in the chemical bonds of the praseodymium ion. *J Chem Phys* 39: 786–793, 1963.
 107. HH Caspers, HE Rast, RA Buchanan. Energy levels of the Pr^{3+} in LaF_3 . *J Chem Phys* 43: 2124–2128, 1965.
 108. E Loh. Ultraviolet absorption spectra of Pr^{3+} ion in alkaline-earth fluorides. *Phys Rev* 158: 273–279, 1967.
 109. WM S Heaps, LR Elias, WM Yen. Vacuum-ultraviolet absorption bands of trivalent lanthanides in LaF_3 . *Phys Rev B* 13: 94–104, 1976.
 110. LR Elias, WM S Heaps, WM Yen. Excitation of uv fluorescence in LaF_3 doped with trivalent cerium and praseodymium. *Phys Rev B* 8: 4989–4995, 1973.
 111. WW Piper, JA De Luca, FS Ham. Cascade fluorescent decay in Pr^{3+} -doped fluorides: achievement of a quantum yield greater than unity for emission of visible light. *J Lumin* 8: 344–348, 1974.

112. AM Srivastava, DA Doughty, WW Beers. On the vacuum-ultraviolet excited luminescence of Pr^{3+} in LaB_3O_6 . *J Electrochem Soc* 144: L190–L192, 1997.
113. AM Srivastava, WW Beers. Luminescence of Pr^{3+} in SrAl_2O_9 ; observation of two photon luminescence in oxide lattice. *J Lumin* 71: 285–290, 1997.
114. AM Srivastava, DA Doughty, WW Beers. Photon cascade luminescence in Pr^{3+} in $\text{LaMgB}_5\text{O}_{10}$. *J Electrochem Soc* 143: 4113–4116, 1997.
115. KM Devyatkova, ON Ivanova, SA Oganessian, KB Seiranyan, SP Chernov. Luminescent properties of single crystals of $\text{LiYF}_4:\text{Nd}^{3+}$ in the vacuum ultraviolet region. *Sov Phys Dokl* 35: 56–57, 1990.
116. GJ Quarles, GE Venikouas, RC Powell. Sequential two-photon excitation processes of Nd^{3+} ions in solids. *Phys Rev B* 31: 6935–6940, 1985.
117. J Sugar. Analysis of the third spectrum of praseodymium. *J Opt Soc Am* 53:831–839, 1963.
118. MA Dubinskii, NM Khaidukov, IG Garipov, LN Dem'yanets, AK Naumov, VV Semashko, VA Malysov. Spectral–kinetic and laser characteristics of new Nd^{3+} -activated laser hosts of the $\text{KF}-\text{YF}_3$ system. *J Mod Opt* 37: 1355–1360, 1990.
119. W Baer, JG Conway, SP Davis. Crystal spectrum of promethium $^{3+}$ in LaCl_3 . *J Chem Phys* 59: 2294–2302, 1973.
120. SIJ Weissman. Intermolecular energy transfer. The fluorescence of complexes of Euro *J Chem Phys* 10: 214–217, 1942.
121. M Schlesinger, T Szcurek. Vacuum ultraviolet spectra of $\text{CaF}_2:\text{Eu}^{3+}$ and $\text{CaF}_2:\text{Sm}^{3+}$. *J Opt Soc Am* 70: 1025–1029, 1980.
122. HE Rast, JL Fray, HH Caspars. Energy levels of Sm^{3+} in LaF_3 . *J Chem Phys* 46: 1460–1466, 1967.
123. JD Axe, GH Dieke. Calculation of crystal field splittings of Sm^{3+} and Dy^{3+} levels in LaCl_3 with inclusion of J mixing. *J Chem Phys* 37: 2364–2371, 1962.
124. BP Zakharchenya, VP Makarov, A Ya Ruskin. Zeeman effect for d-f transitions in the spectra of Sm^{2+} activated alkali-earth fluoride crystals. *Opt Spect* 17: 116–120, 1964.
125. ZJ Kiss, HA Weakliem. Stark effect of 4f states and linear crystal field in $\text{BaClF}:\text{Sm}^{2+}$. *Phys Rev Lett* 15: 457–460, 1965.
126. BP Zakharchenya, AYa Ruskin. Zeeman effect in the absorption and luminescence spectrum of $\text{CaF}_2:\text{Sm}^{++}$ and $\text{SrF}_2:\text{Sm}^{++}$ crystals. *Opt Spect* 13: 501–502, 1962.
127. E Loh. $4f^n \rightarrow 4f^{n-1}5d$ spectra of rare-earth ions in crystals. *Phys Rev* 175: 533–536, 1968.
128. RT Wegh, H Donker, A. Meijerink. Vacuum ultraviolet excitation and emission studies of $4f^n \rightarrow 4f^{n-1}5d$ transitions for Ln^{3+} in LiYF_4 . *Proc Elect Soc* 97: 284–295, 1988.
129. M Schlesinger, GFW Drake. On the vibronic spectrum of rare-earths in calcium fluoride. *Can J Phys* 54: 1699–1701, 1976.
130. WC Martin, R Zalubas, L Hagan. Atomic Energy Levels—The Rare Earth Elements. Washington, DC: National Bureau of Standards, 1978.
131. J Sugar, J Reader. Ionization energies of doubly and triply ionized rare earths. *J Chem Phys* 59: 2083–2089, 1973.
132. JF Kielkopf, HM Crosswhite. Preliminary analysis of the spectrum of triply ionized gadolinium (Gd IV). *J Opt Soc Am* 60: 347–351, 1970.

133. GH Dieke. In: Crosswhite HM, Crosswhite H, eds. *Spectra and Energy Levels of Rare Earth Ions in Crystals*, New York: Wiley, 1968, pp 249–253.
134. M Schlesinger, T Szczurek, GWF Drake. The lowest energy $4f \rightarrow 5d$ transition of the triply ionized gadolinium in CaF_2 . *Solid State Commun* 28: 165–166, 1978.
135. E Sarantopoulou, AC Cefalas, MA Dubinskii, Z Kollia, CA Nicolaidis, RY Abdul-sabirov, SL Korableva, AK Naumov, VV Semashko. VUV and UV fluorescence and absorption studies of Tb^{3+} and Tm^{3+} trivalent ions in LiLuF_4 single crystal hosts. *J Mod Opt* 41: 767–775, 1994.
136. JL Fray, HH Caspars, HE Rast, SA Miller. Optical absorption and fluorescence spectra of Dy^{3+} in LaF_3 . *J Chem Phys* 48: 2342–2348, 1968.
137. M Schlesinger, T Szczurek, MCK Wiltshire. $4f \rightarrow 5d$ transition studies of Tb^{3+} and Dy^{3+} in calcium fluoride. *Can J Phys* 54: 753–756, 1975.
138. T Szczurek, M Schlesinger. $4f \rightarrow 5d$ transition studies of Ho^{3+} in calcium fluoride. *Phys Rev B* 9: 3938–3940, 1974.
139. AA Vlasenko, LI Devyatkova, ON Ivanova, VV Mizailin, SP Chernov, T Uvarova, BP Sobolev. Transmission spectra of single crystals of the type BaLn_2F_8 in a wide spectral region (from 12 to 0,12 μm). *Sov Phys Dokl* 30: 395–397, 1985.
140. LI Devyatkova, ON Ivanova, VV Mikhailin, SN Rudnev, BP Sobolev, TV Uranova, SP Chernov. Experimental study of $4f$ - $5d$ transitions in Ho^{3+} , Er^{3+} , Tm^{3+} , and Yb^{3+} in BaY_2F_8 . *Sov Phys Dolk* 30: 687–689, 1985.
141. KM Devyatkova, ON Ivanova, KB Seiranyan, SA Tamazyan, SP Chernov. Vacuum ultraviolet properties of a new fluoride matrix. *Sov Phys Dokl* 35: 40–41, 1990.
142. LI Devyatkova, ON Ivanova, VV Mikhailin, SN Rudnev, SP Chernov. High energy $4f$ states of Er^{3+} and Ho^{3+} ions in fluoride crystals. *Sov Phys Dolk* 62: 275–276, 1985.
143. T Szczurek, M Schlesinger. Spectroscopic studies of excited Tm^{3+} ions in CaF_2 crystals. *Phys Rev B* 34: 6109–6111, 1986.
144. M Schlesinger, T Szczurek. Spectroscopic studies of excited Tm^{3+} ions in alkaline-earth fluorides. *Phys Rev B* 35: 8341–8347, 1986.
145. T Szczurek, M Schlesinger. Temperature dependent rare-earth impurity-site symmetries in CaF_2 . *Phys Rev B* 36: 8263–8267, 1987.
146. BW Bryant. Spectra of doubly and triply ionised Ytterbium YbIII and Yb IV. *J Opt Soc Am* 55: 771–779, 1965.
147. M Schlesinger, T Szczurek, MK Wade, GWF Drake. Anomalies in the vacuum uv absorption spectrum of Yb^{3+} in CaF_2 . *Phys Rev B* 18: 6388–6390, 1978.
148. E Loh. Ultraviolet-absorption spectra of europium and ytterbium in alkaline earth fluorides. *Phys Rev B* 184: 348–352, 1969.
149. E Loh. Strong-field assignment on $4f^{13}5d$ levels of Yb^{2+} in SrCl_2 . *Phys Rev B* 7: 1846–1850, 1972.
150. RT Wegh, H Donker, A Maijerink. Spin-allowed and spin-forbidden fd emission from Er^{3+} and LiYF_4 . *Phys Rev B* 57: R2025–R2028, 1998.
151. MB Seelbinder, JC Wright. Site selective spectroscopy of $\text{CaF}_2:\text{Ho}^{3+}$. *Phys Rev B* 20: 4308–4320, 1979.
152. E Sarantopoulou, YS Raptis, E Zouboulis and C Raptis. Pressure and temperature-dependent Raman study of YLiF_4 . *Phys Rev B* 59: 4154–4162, 1999.
153. P Dorenbos, CWE van Eijk, AJJ Bos, CL Melcher. Scintillation and thermolumi-

- nescence properties of $\text{Lu}_2\text{SiO}_5:\text{Ce}$ fast scintillation crystals. *J Lumin* 60&61: 979–982, 1994.
154. O Guillot-Noël, JTM de Haas, P Dorenbos, CWE van Eijk, K Krämer, HU Güdel. Optical and scintillation properties of cerium-doped LaCl_3 , LuBr_3 and LuCl_3 . *J Lumin* 85:21–35, 1999.
 155. JC van't Spijker, P Dorenbos, CWE van Eijk, K Krämer, HU Güdel. Optical and scintillation properties of Ce^{3+} doped K_2LaCl_5 . *J Lumin* 85: 1–10, 1999.
 156. CM Combes, P Dorenbos, CWE van Eijk, K Krämer, HU Güdel. Optical and scintillation properties of pure and Ce^{3+} -doped $\text{Cs}_2\text{LiYCl}_6$ and $\text{Li}_3\text{YCl}_6:\text{Ce}^{3+}$ crystals. *J Lum* 82: 299–305, 1999.
 157. O Guillot-Noël, JC van't Spijker, JTM de Haas, P Dorenbos, CWE van Eijk, K Krämer, HU Güdel. Scintillation properties of $\text{RbGd}_2\text{Br}_7:\text{Ce}$: advances and limitations. *IEEE Trans Nucl Sci* 46: 1274–1284, 1999.
 158. EG Devitsin, N Yu Kirikova, VA Kozlov, VN Makhov, S Yu Potashov, LN Dmitruk, MA Terekhin, IH Munro, C Mythen, DA Shaw, KW Bell, RM Brown, PS Flower, PW Jeffreys, JM Parker. Time-resolved studies of emission properties of cerium-doped fluoro-hafnate glasses under VUV synchrotron radiation excitation *Nucl Instr Methods Phys Res A*405: 418–422, 1998.
 159. P Dorenbos, JC van't Spijker, OWV Frijns, O Guillot-Noël, CWE van Eijk, K Krämer, HU Güdel, A Ellens. Scintillation properties of $\text{RbGd}_2\text{Br}_7:\text{Ce}^{3+}$ crystals; fast efficient and high density scintillators. *Nucl Instr Methods Phys Res B*132: 728–731 1999.
 160. CM Combes, P Dorenbos, CWE van Eijk, C Pedrini, HW Den Hartog, JY Gesland, PA Rodnyi. Optical and scintillation properties of Ce^{3+} doped LiLuF_4 and LiLuF_4 crystals. *J Lumin* 71: 65–70, 1997.
 161. MA Dubinskii, VV Semashko, AK Naumov, R. Yu Abdulsabirov, S Korableva. Ce^{3+} doped colquirite. A new concept of all-solid state tunable ultraviolet laser. *J Mod Opt* 40: 1–5, 1993.
 162. C Combes. Scintillation properties of ^6Li -based materials for thermal-neutron detection. PhD thesis, Technical University of Delft, 1999.
 163. S Nicolas, Y Guyot, VV Semashko, R Yu Abdulsabirov, E Descoix, MF Joubert. Spectroscopie de l'ion Pr^{3+} dans LiLuF_4 . Proceedings, Phenomenes Luminescents des Materiaux Isolants, Lyon, France, 1999.
 164. SA Payne, GD Wilke. Transient gratings by 4f to 5d excitation of rare earth impurities in solids. *J Lumin* 50: 159–168, 1991.
 165. RB Barthem, R Buisson, JC Vial, H Harmand. Optical properties of Nd^{3+} pairs in LiYF_4 -existence of a short range interaction. *J Lumin* 34: 295–305, 1986.
 166. M Grwe, S Tavernier. Determination of the scintillation light yield of neodymium doped LaF_3 scintillator. *Nucl Instr Methods Phys Res A*311: 301–305, 1992.
 167. P Dorenbos, JTM de Haas, CWE van Eijk. The intensity of the 173 nm emission of $\text{LaF}_3:\text{Nd}^{3+}$ scintillation crystals. *J Lumin* 69: 229–233, 1996.
 168. AN Belsky, P Chevallier, JY Gesland, N Yu Kirikova, JC Krupa, VN Machov, P Martin, PA Orekhanov, M Queffelec. Emission properties of Nd^{3+} in several fluoride crystals. *J Lumin* 72/74: 146–148, 1997.
 169. MA Dubinskii, R Yu Abdulsabirov, SL Korableva, AK Naumov, VV Semashko.

- On the possibility of ultraviolet lasing on f-f transitions in Nd^{3+} ion. *Laser Phys* 2: 239–241, 1992.
170. MA Dubinskii. Light-driven optical switch, based on excited state absorption in activated dielectric crystals. *J Mod Opt* 38: 2323–2326, 1991.
 171. WM Yen, PM Selzer. *Laser Spectroscopy of Solids*. Berlin: Springer Verlag, 1981.
 172. RT Wegh, H Donker, A Meijerink. Spin allowed and spin-forbidden fd emission from Er^{3+} in LiYF_4 . *Phys Rev B* 57: R2025–R2028, 1998.
 173. RT Wegh, A Meijerink. Spin-allowed and spin-forbidden $4f^n \rightarrow 4f^{n-1}5d$ transitions for heavy lanthanides in fluoride hosts. *Phys Rev B* 60: 10820–10830, 1999.
 174. AC Cefalas, Z Kollia, E Sarantopoulou. Vacuum Ultraviolet $4f^95d \rightarrow 4f^{10}$ interconfigurational transitions of Ho^{3+} ions in LiLuF_4 single crystals. *J Opt Soc Am B* V16: 625–630, 1999.
 175. E Sarantopoulou, Z Kollia, AC Cefalas. $4f^95d \rightarrow 4f^{10}$ spin-allowed and spin-forbidden transitions of Ho^{3+} ions in LiYF_4 single crystals in the vacuum ultraviolet. *Opt Commun* 169: 263–274, 1999.
 176. J Becker, JY Gesland, M Yu Kirikova, JC Krupa, VN Makhov, M Runne, M Queffelec, TV Uvarova, G Zimmerer. Fast VUV emission of rare earth ions (Nd^{3+} , Er^{3+} , Tm^{3+}) in wide band gap crystals. *J Alloys Comp* 275–277: 205–208, 1998.
 177. A Meijerink, RT Wegh. VUV spectroscopy of lanthanides: extending the horizon. *Materials Sci Forum* 315–317: 11–26, 1999.
 178. JC Krupa, M Queffelec. UV and VUV optical excitations in wide band gap materials doped with rare earth ions: $4f-5d$ transitions. *J Alloys Comp* 250: 287–292, 1997.
 179. P Dorenbos. The $5d4f^{n-1} \rightarrow 4f^n$ luminescence of trivalent rare earth ions in inorganic crystals. *Materials Sci Forum* 315–317: 222–227, 1999.